Department of Precision and Microsystems Engineering

Manipulating the stiffness of post-buckled beams using topology optimization

Rajiv Randy Kapildewsing

Report no	:	2021.095
Coach	:	T.W.A Blad
Professor	:	J.L. Herder
Specialisation	:	MSD
Type of report	:	M.Sc. Thesis
Date	:	19 November 2021

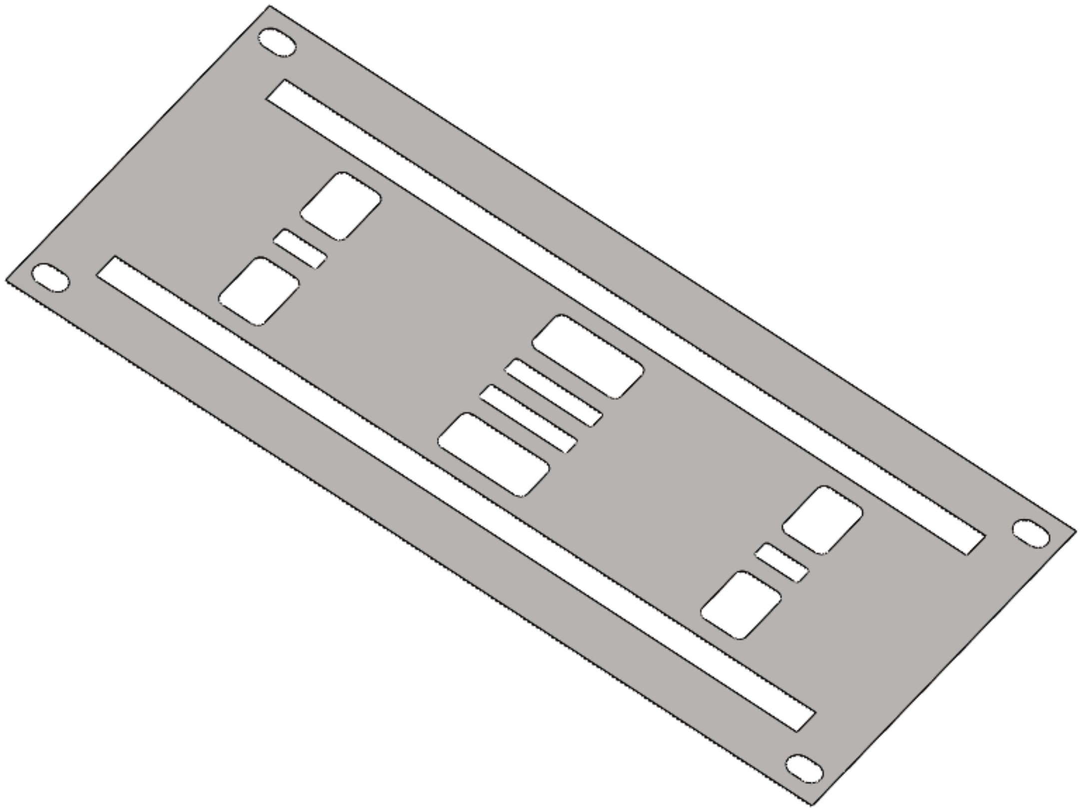

TU Delft Delft University of Technology

Manipulating the stiffness of post-buckled beams using topology optimization

Manipulating the stiffness of post-buckled beams using topology optimization

M.Sc. Thesis

In partial fulfilment of the requirements for the degree of
Master of Science in Mechanical Engineering.
Department of Precision and Microsystems Engineering.
Delft University of Technology, Delft, The Netherlands.
To be defended on Friday December 3th, 2021 at 14:30.

by

Rajiv Randy KAPILDEWSING

born in Amsterdam, The Netherlands.

Report no.	2021.095
Coach	T.W.A Blad
Professor	J.L. Herder
Specialization	MSD
Type of report	M.Sc. Thesis
December 3,	2021

This thesis was approved by the thesis committee:

Prof. dr. ir. J.L. Herder,	PME, 3ME, TU Delft
dr. ir. T.WA. Blad,	PME, 3ME, TU Delft

Keywords: Compliant mechanisms, buckling, vibration energy harvesting

Printed by:

Cover:

An electronic version of this thesis is available at
`http://repository.tudelft.nl/`.

Preface

As a kid I always loved cars, I was able to name every brand and model I could see on the streets without hesitation. When I became older I began to question why cars can move like they do. Later I started middle school I still did not found a satisfactory explanation. This was simply because the internal combustion engine and other parts of a car were far more complicated that I could ever imagine at that age. Then it became clear I had to study mechanical engineering because this would explain all the different machines and structures I saw outside. During my bachelor's study I actually lost interest in cars but gained so much more interest in other fields of engineering. I began to realise that every machine is far more complex than I could imagine. Things being complex or difficult to understand always peaked my interest for some reason.

During my master's I learned about energy harvesting and I knew immediately that this was something I wanted to do. The fact that it can possibly help people with their pacemakers, or hearing aids made this decision very easy. Even though energy harvesters probably will not see any use in the near future, I just loved the challenges of this engineering project. Searching for solutions in non-linear mechanisms, which are normally avoided, made this graduation project a perfect fit for me.

Rajiv
Amstelveen, November 2021

Summary

Vibration energy harvesters can help in different areas. These vary from supplying power to medical implants or wireless sensors that can aid in predicting natural disasters. However, the problem is that they are not able to generate power across a large bandwidth of frequencies. Bistable energy harvesters can solve this problem when these are able to oscillate between their stable equilibria. A bistable mechanism that has these benefits is a post-buckled beam. However, a potential energy barrier needs to be overcome before this interwell motion can occur. If there is no interwell motion, the power output will be severely reduced. Using buckling load matching the potential barrier can be lowered. The apparent potential barrier that has to be overcome is the difference between the total strain energy in the first- and second buckling mode. The difference between the buckling loads are also indicators of the difference of strain energy between the two buckling modes. A topology optimization is performed on a slender beam so that the buckling loads approach almost equality. This leads to lowering of the potential barrier and thus interwell motion is eased. In this topology optimization the second buckling load was lowered, whilst maintaining the first buckling load and therefore lowering the potential barrier. The buckling loads are calculated using finite element modelling. Another topology optimization is done on the slender beam where the opposite is done. An endeavour is made to lower the first buckling load, whilst maintaining the second buckling load. This increases the potential barrier and this stiffens the post-buckled beam. The force-deflections from the two different designs are numerically simulated and these are experimentally verified. This shows that is possible to target reduce either one of the first two buckling loads. Doing this can lead to reducing or increasing the stiffness of a post-buckled beam. The method provided can be a useful tool to manipulate the stiffness of post-buckled beams in both directions.

Contents

1 Introduction

In this chapter an introduction is given on the overarching topic vibration energy harvesting. The basic principles are explained and possible future applications are presented. Then different performance improvement techniques are shown. This introduces the problem statement and research goal of this thesis. Also the structure of the thesis is outlined.

1.1 Energy harvesting

Energy is a vital part of modern society. Most of the energy resources worldwide now come from fossil fuels [1]. Renewable energy is getting more attention due to its low carbon footprint and is a prime example of modern day energy harvesting. Windmill, solar panels, geo thermal power plants and hydro dams are all forms of energy harvesting. Energy from the environment is converted to (mainly) electrical energy. The energy sources can differ to be from the kinetic energy from the wind/water or from heat. These forms of energy harvesting are mainly large scale and meant to power the grid.

But energy harvesting can also be found on smaller scales. Modern hybrid F1 cars also use energy harvesting to improve performance. When a car brakes, kinetic energy is lost and converted to heat. F1 cars have units that are able to convert this heat into electrical energy, a similar unit is also used to capture energy from the hot exhaust fumes and convert this also into electrical energy. The electrical energy is then used to charge a battery, this battery delivers energy to the electrical motor which is able to deliver 120 kW of power. Because of this F1 cars have a thermal efficiency of around 50%, that is more than double of a regular road car which has a thermal efficiency around 20% [2]. This shows how powerful it can be to harvest otherwise considered useless energy.

A lot of energy is wasted in the form of vibrations. Structures such as buildings, bridges or other mechanical structures that are influenced by air flow vibrate. Converting this energy into useful electrical energy is what vibration energy harvesters are made for. The otherwise considered useless energy can be converted to something useful. This allows for smaller electronics to be supplied with electrical energy from normally wasted energy.

And in our daily life we are dependent on smaller electronics. This could be a hearing aid, a watch and other devices with low energy consumption. These devices are reliant on batteries for their supply of electrical energy. These batteries either need to be recharged or replaced. It can be cumbersome to replace some batteries, for example in medical implants such as spinal simulators or pacemakers. Vibration energy harvesters have the advantage that they are able to produce electrical energy locally, making it possible to have a medical implant that might never need replacement. Also batteries need to be disposed after replacement, this has an adverse effect on the environment [3].

1.1.1 Applications and relevance

The disadvantages of batteries can be circumvented using vibration energy harvesters. Vibrations are roughly said to be energy sources that can not be depleted. Using vibration energy harvesters to charge batteries would allow to reduce maintenance or even completely replace them. Vibration energy harvesting is a great candidate to aid in *wireless sensor networks* [4]. These sensors can monitor the integrity of different structures. They need to be in hard-to-reach places, making maintenance difficult. The sensors always need to be functioning making long up-time desirable.

Wireless sensor networks can aid in many different fields. In 2020 there were massive forest fires in Australia killing flora and fauna. Using wireless sensors it is possible to monitor temperature, humidity and gases that are produced by fire. This allows for quick pinpointing of the origin of the fire, letting the fire brigade have a bigger chance of containing the fire [5, 6].

Natural disasters will always happen making early detection life saving. Using wireless sensors many different natural disasters can be detected, such as floods, forest fires and landslides [7].

Using vibration energy harvesters in portable devices are also possible applications. There are already watches available without batteries, these need to be charged by swinging your wrist. Other possible devices that can benefit are medical implants. Battery replacement of these implants requires surgery and therefore risks are involved. By applying vibration energy harvesters these surgeries can be postponed and in an ideal world, be completely obsolete.

1.2 Fundamentals of vibration energy harvesting

Vibrations are everywhere, making harvesting their energy attractive. There are many sources from which energy can be harvested such as: human motion, vibrations of bridges, wind across structures. These are sources which usually dissipate into heat, but using vibration energy harvesters this energy is converted to usable electric power.

1.2.1 Working principle

To harvest energy from vibrations, these vibrations need to be 'captured'. This is done by letting a mechanism oscillate due to incoming vibrations. This kinetic energy still needs to be converted to electrical energy. This is done using transduction mechanisms: piezoelectric, electromagnetic and electrostatic. These transduction mechanisms couple the mechanical and electromechanical domain [8]. To optimize the energy output, large accelerations and large amplitude motion is needed from the mechanism. To achieve this most vibration energy harvesters are designed to resonate due to the incoming vibrations [9]. An example is shown in Fig. 1.1, this mechanism uses a piezoelectric layer as a transduction mechanism.

However, these mechanisms resonate only at certain frequencies. If the mechanism does not resonate, power output is massively decreased. This makes them unpractical, because in real-world applications vibrations are not a single frequency. Vibrations in the real-world mostly exhibit multiple frequencies which can change over time [10]. This makes vibration energy harvesters unreliable. To improve the reliability in the real-world

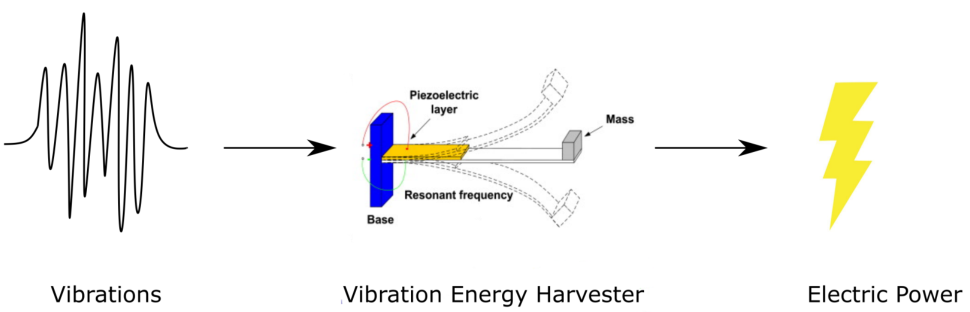

Figure 1.1: Steps to convert vibrations to electrical power

the *bandwidth* needs to be improved. The bandwidth is the operation window of frequencies where the harvester can produce usable power output. Bandwidth is the main limitation for vibration energy harvesters to be used in real-world applications.

1.2.2 Techniques to improve bandwidth

To solve the bandwidth problem different techniques can be used, these are mainly non linear.

A Duffing non linearity can be introduced in the system, this will bent the resonance peak. This can widen the bandwidth of the vibration energy harvester. However, this introduces multiple solutions for one frequency. This is shown in Fig. 1.2a. It is preferred to have the high amplitude solution, but this cannot be guaranteed. This is dependent on whether the incoming vibration are in increasing or decreasing frequency.

An interesting non linearity that can be induced is internal resonance. The presence of internal resonances in the system can increase the bandwidth by generating different branches around the primary resonance frequency. This is shown in Fig. 1.2b. This however increases the needed excitation levels of the incoming vibration to function. This generally makes internal resonance harvesters less efficient than their linear counterpart [11].

A non linear technique that can improve the bandwidth is bi stability. An example which will be thoroughly be researched in this thesis, is a beam in its post-buckled state. These mechanisms can have large interwell oscillations if the excitation amplitude is large enough. The advantage of these mechanisms is that these interwell oscillations can occur at a broad band of frequencies, meaning that the bandwidth of can be significantly improved. The disadvantage is however that when the amplitude of the incoming vibration is not high enough to establish interwell motion, power output is massively reduced. Designing these mechanisms requires knowledge of excitation levels from the incoming vibrations.

A relatively new development in bandwidth improvement is the mechanical stopper technique. In most cases, stoppers are placed on either side of a cantilever beam. When the beam oscillates, it hits the mechanical stoppers. This causes the stiffness to increase upon impact, this changes the eigenfrequency and causes a broadening in the bandwidth. However, the maximum amplitude of the cantilever beam is reduced, which reduces the power output.

When miniaturizing vibration energy harvesters, another problem raises. The smaller a harvester gets, the higher its resonance frequency will be. However, most useful vibration sources are low frequency. This makes it difficult to harvest electrical energy on small scale. To resolve this issue, frequency-up conversion is used [12]. There are two oscillators coupled to each other, a low- and high-frequency oscillator. The low frequency oscillator is designed so that it will oscillate due to the incoming low frequency vibrations. Due to the coupling the high-frequency oscillator will oscillate at its resonance frequency. This makes it possible for harvesters on a small scale to have relatively large power output.

All these techniques can be used to improve the bandwidth of vibration energy harvesters and therefore improve the power output in real word scenarios. But there is no clear-cut best technique. Each technique brings disadvantages and should be carefully chosen for a certain application. In the current state there is no general solution to solve

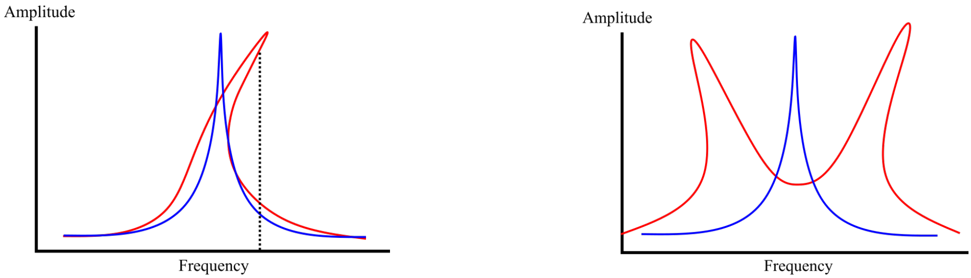

(a) Duffing non linearity compared to a linear system. Duffing non linearity introduces multiple solutions at certain frequencies.

(b) Internal resonance system compared to linear system. Internal resonance introduces 'double branching' which improves the bandwidth.

Figure 1.2: Non linear systems compared to linear systems

the bandwidth problem. It is therefore important to know beforehand the excitation frequencies and amplitude. This will allow for a vibration harvester to be designed for a specific application using appropriate bandwidth improving techniques [13].

1.3 Thesis structure

The main line of research of this thesis is stiffness influencing in post-buckled beams. Influencing the stiffness in post-buckled beams will allow for a larger design space. This will allow post-buckled beams to be designed for different scenario's. Two other topics are also touched upon: Internal resonance in vibration energy harvesters and topology optimization used in post-buckled beams.

In Chapter 2 the resulting paper of the literature review phase is presented. In this review an extensive overview is given on internal resonance as a solution to the bandwidth problem. The non linear phenomena is explained and the needed conditions are summarised. A classification is given of the the different types of internal resonance harvesters. Each type is then compared using certain metrics.

Chapter 3 is an introduction to the research hypothesis. A hypothesis is formulated based on the findings in the literature review and the necessary tools that are needed to support this hypothesis are presented.

Chapter 4 presents the research paper on stiffness influencing using topology optimization. The hypothesis is tested using finite element models. Prototypes are also made and these are experimentally tested to validate the numerical model and hypothesis. This results in a framework that can be used to influence stiffness of post-buckled beams in both directions. Meaning it is possible to reduce stiffness and stiffen the post-buckled beam by removing material at the right places.

In Chapter 5 a critical reflection is given of the author of the work and process. Conclusions are presented and recommendations are given for future work.

In appendix A a detailed explanation of the build software that was used in the topology optimization is presented. Also the finite element model that was used to peform this optimization is also shown.

In appendix B the technical drawings are given of all the manufactured designs.

Appendix C shows the result of a topology optimization where stiffness is maximized. In this optimization process further improvements are made to the design found in chapter 4. The optimization is improved by increasing the amount of elements in the finite element model.

2

Internal resonance in energy harvesting

In this chapter the paper that was written during the literature review phase is shown. The research paper concerns a certain technique used to improve the performance of vibration energy harvesters. It classifies all the different mechanisms that use this technique. Using these classifications the performance of each class is evaluated.

2.1 Introduction

Harvesting energy from the environment is human nature and is mandatory in modern society. In today's world it is mostly known in the forms of solar panels and windmills. These constructions convert ambient energy to electric power and is supplied to the power grid. The examples mentioned are on a large scale, energy harvesting is also prominent on small scale. A typical example is the dynamo of a bicycle, the dynamo converts human power to electrical power for supplying the lights.

In the last decade a lot of research is focused on harvesting energy from environmental vibrations. Vibration energy harvesters(VEHs) can be used in different fields such as structure monitoring, environmental monitoring and medical implants. Structural and environmental monitoring can be improved using wireless sensor networks. The sensors can be used to monitor the condition of a structure or the environment (e.g., air pollution, CO_2 concentration) and improve public safety. Medical implants benefit from the reduction in surgeries.

In current research internal resonance has gotten attention in vibration energy harvesting. Internal resonance is a nonlinear phenomenon that can occur when two resonant frequencies are commensurate. If internal resonance in a system occurs, one of the excited modes is able to exchange energy with another mode. Because of this interaction the amplitude response changes of the system, a so called 'coupled mode response' [14]. The interaction between the modes does not necessarily help in energy harvesting (it is possible and examples will be discussed in Section IV). However, what does help is the changing nonlinear characteristics of the system. When internal resonance occurs it can change the behaviour of the system such that the amplitude follows the direction of the frequency in both ways. In other words, the response has both a hardening and softening response, this can improve the bandwidth in energy harvesters.

Another interesting mechanic of internal resonance is apparent when the system is harmonically excited at its resonant frequency. The internal resonant system will exhibit two frequency peaks in its FFT, due to the coupling of the modes.This is shown by Emam et. al. where they researched the non linear response of buckled beams [15]. This behaviour can be used to implement frequency up-conversion. Wu et. al. [16] studied an internal resonance frequency up-converting harvester. They found that is is certainly possible but a 'huge size and flimsy' structure that is needed makes it easily breakable. In literature the ratio of the first and second eigenfrequencies are often noted as 2:1, meaning that the second eigenfrequency is two times the first eigenfrequency.

However, in current research the bandwidth of the VEH's is a limiting factor to allow applications in the real world. Multiple design parameters of the cantilever beam can be varied so that the resonance frequency is close to the excitation frequency. The performance of the VEH is reduced drastically when it is not resonating. The bandwidth at which a linear harvester can operate is very small, this is the main drawback of linear VEHs. In reality, excitations are not perfectly harmonic but rather are widely spread over a range of frequencies. Because of the narrow bandwidth it is also difficult to manufacture, small deviations of a design parameter can detune the resonance frequency.

In order to solve the bandwidth problem in VEHs, nonlinear techniques have been used to combat this problem. With the use of nonlinear techniques the operational bandwidth can be improved. Typical nonlinear responses are Fig. 2.1a-2.1b. Thus the VEH can than

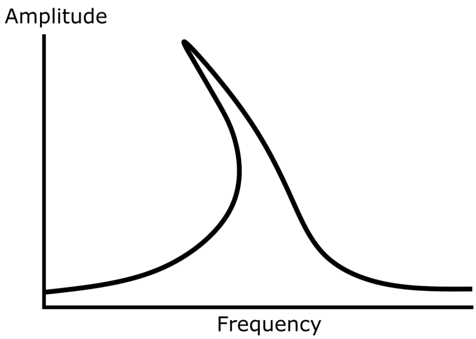

(a) Softening response

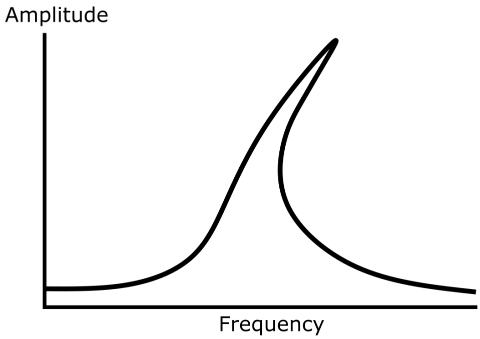

(b) Hardening response

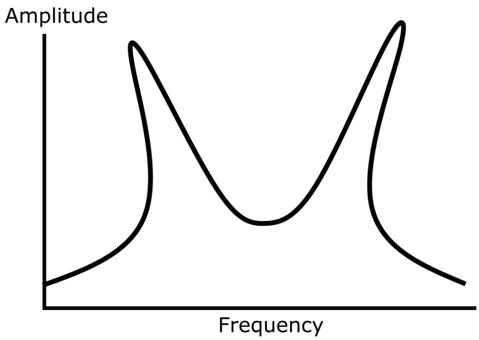

(c) Internal resonance response

Figure 2.1: The internal resonance response has both characteristics of the hardening and softening response.

possibly generate more power in practical applications, where environmental excitations are spread over a larger range of frequencies.

In this paper a focus is made on internal resonance in VEH's. A generic response of such an internal resonance harvester is shown in Fig. 2.1c. From this figure it can be seen how the double bending can lead to bandwidth improvement. The research objective of this work is to give an insight of the current internal resonance energy harvesters in literature. This will be done by depicting the different concepts that can achieve internal resonance. The rich dynamics some of these concepts can have will be discussed. The power and bandwidth are also compared for the different harvesters. In section II the method used to compare the different internal resonance VEH's in literature is presented. Then it will be shown which methods are used to enforce internal resonance in a VEH in section III. In section IV an overview is given of the different VEH's and how they compare to each other. And lastly a discussion is presented and conclusions are drawn in the last section.

2.2 Methods

In order to make any comparison it is important to define 'bandwidth'. There are multiple ways to measure bandwidth. Nonlinear responses can have multiple solutions for the same frequency. In order to take that into account A Cammarano et al. introduced the maximum/power solution method[17]. However, such definitions need the knowledge of unstable branches which are not measured in the real world. For that reason the standard *3-dB bandwidth* will be used.The bandwidth is then defined as the maximum amplitude and take half the value. Every frequency that is above this amplitude value is considered within the bandwidth. There are papers that only give simulations and numerical validations, these will be mentioned and the findings in those papers will be reported.

In order to compare the bandwidth of the VEH's it is important that the bandwidth obtained using this definition is relative. If a VEH has a resonance frequency of 10 kHz and has a bandwidth of 2 Hz, it is comparatively small., whilst this bandwidth is relatively high if the resonance frequency is 10 Hz. To compare, a dimensionless bandwidth introduced by Mitcheson is used[18]:

$$FoMBW = \frac{\omega_{3dB}}{\omega_1} \tag{2.1}$$

2.2.1 Data aquisition

In order to compare different VEH's it is important to do it fairly. This is done by using certain definitions that will be made in this section. Firstly, the mass of a VEH is in this review defined as the mass of the flexures, proof masses and magnets. This does not contain the masses used for energy conversion, such as piezoelectric members and coils. The 3dB bandwidth definition does not give a insight in the complex behaviour of a VEH that utilises internal resonance. Because of nonlinear behaviour the VEH responds differently when the frequency-sweep is done upward or downwards. This can be important in certain applications. In order to utilise a internal resonance VEH it is important to know certain characteristics of the excitations. For example, if the VEH is gonna be applied on a car engine it is known beforehand that it will generally not be lower than 1000 rpm. The excitation most likely will have a 'frequency up sweep behaviour'. A VEH that performs better in a frequency up sweep will therefore perform better in such a situation.

In order to give insight in this behaviour the bandwidth of the up and down sweep are given. However, a VEH might have better bandwidth on a up-sweep, but this does not necessarily mean that it performs better. To compare the output the integral of the frequency-voltage plot are compared. This metric is the most consistently reported in the found literature to allow comparison. This integral is evaluated for the up and down sweep and divided by each other, this metric will be called the Sweep Figure of Merit (SFoM). This metric gives a insight of the behaviour of the VEH, it tells whether the output over a certain frequency range is better or not.

In order to evaluate the SFoM equation 2.2 is used. A negative number will represent that the performance of the down sweep is better whilst a positive number will be for a up sweep. The magnitude of the number will then show how much difference there is between the up- and down sweep.

$$SFoM = \left|100 - \frac{\int Upsweep}{\int Downsweep} * 100\right| \tag{2.2}$$

Now that the general behaviour of the VEH is described in numbers, the maximum power output also needs to be compared. This needs to be done in a fair manner since a VEH can obviously harvest more energy when the excitation accelerations are higher. Same can be said over the mass, if the VEH has more mass it is also able to harvest more energy. The PNMA is given by Liu et al. [19] and defined as :

$$PNMA = \frac{P}{M\gamma_0^2} \tag{2.3}$$

2.3 Classifications

Internal resonance can be achieved in multiple manners. In order to achieve it, the system needs to be nonlinear (at least a cubic nonlinearity) and the frequencies of two modes need to (closely) commensurate. Different geometry can be chosen to induce internal resonance and will be discussed. In literature the main geometry concepts are shown in Fig. 2.2. It should also be noted that some concepts include magnets. Magnets are a relatively easy way to implement a nonlinear restoring force into the system. When designed properly the eigenfrequencies of the VEH are dependent on the distance between the interacting magnets. This can make 'frequency-tuning' easier in practice.

2.3.1 Buckled beam

A beam is displaced such that it is in its first buckling mode. By increasing the buckling level of the beam it is possible to induce 3:1 internal resonance in the buckled beam [15]. The main advantage of such a concept is that is 'easily tuned' in practice. This can be simply done by changing the buckling level of the beam. Nayfeh and Emam have done a comprehensive study on internal resonance responses of a buckled beam[15]. Analytical results and illustrations of the responses are given. They also show that when the excitations are high enough there can also be a chaotic response. And they also find that the coupling between the modes is not in both directions. Meaning that when the third mode is excited, the first mode might not be excited (depends on initial conditions). Internal resonance will not occur and the double branching in the frequency response curve will not be there. However, when the first mode is excited they show that the third mode is excited and internal resonance does occur. In energy harvesting it is therefore needed to excite the first resonance frequency to benefit from internal resonance.

2.3.2 L-Shape

Two beams are attached to each other perpendicular to each other to form a L-Shape. Proof masses are applied at the connection between the two beams and at the (closely) top of the vertical beam. It has been shown that for this structure internal resonance can occur [20]. The two modes that are coupled due to internal resonance are the bending modes of the two flexures. So the bending-mode of the vertical beam is coupled with the bending-mode

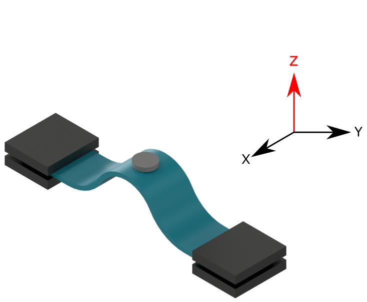

(a) Buckled beam

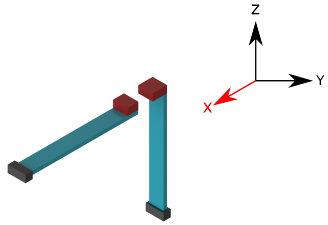

(b) Two beams with magnets

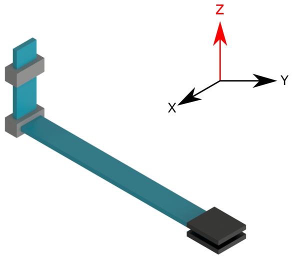

(c) L-Shape

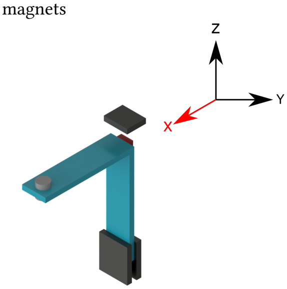

(d) L-Shape with magnets

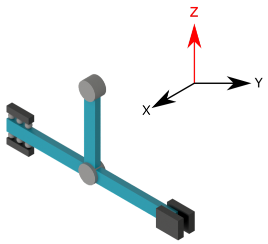

(e) T-Shape

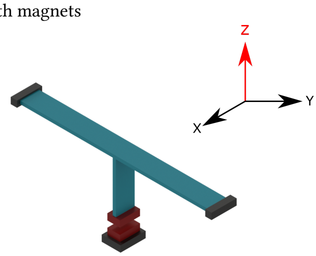

(f) T-Shape with magnets

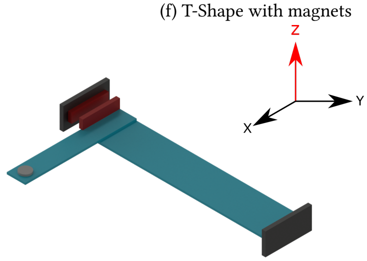

(g) Cantilever with magnets and auxiliary oscillator

Figure 2.2: Classifications of the different internal resonance harvesters. The bases are indicated with black and the direction of the excitations are indicated with red in the coordinate axis.

of the horizontal beam. The coupled modes are in a 2:1 ratio. It has been shown by Nie et. al. that quasi-periodic and chaotic motions can be observed under certain conditions [21].

In order to induce internal resonance the masses and dimensions of the beam need to be carefully chosen. Magnets can be implemented so that the eigenfrequencies of the structure are dependent on the distance between the magnets. The behaviour of the structure also changes and the magnetic interaction also needs to be modelled, making the structure harder to model. The same modes are coupled in the same ratio as in the concept without magnets.

2.3.3 T-Shape

In this concept two beams are connected to form a T-Shape. The two modes that are coupled are also the two bending modes of the beams, as in the L-Shape concept. These are coupled in a 3:1 ratio. The magnets have the same function as in the L-Shape concept. However, it changes the ratio of the modes to 2:1 instead of 3:1 [22].

2.3.4 Two beams with magnets

In this configuration two beams interact with each other due to magnets at the tips. The modes are coupled in a 2:1 ratio. As in the other concepts with magnets, the eigenfrequencies of the system are dependent on the distance between the magnets. The interesting characteristic of this concept however is that the 'double peak' can be tuned. In Fig. 2.1c the two peaks are of the same height in the frequency-amplitude plot. The right branch will increase in peak value whilst the left branch will decrease when the distance between the magnets is increased. When the distance is decreased the left branch will increase whilst the right branch will decrease [23]. This might prove to be useful if the excitation signal is known beforehand. This configuration also allows for frequency up-conversion. This will later be discussed.

2.3.5 Cantilever with magnets and auxiliary oscillator

In this configuration a magnet on the tip of the cantilever beam is placed. This magnet interacts with a stationary magnet, this way the non-linearity for internal resonance is implemented. This itself is not enough to induce internal resonance in practice [24]. It is hard to tune the resonance frequencies to be commensurate, to solve this a linear auxiliary oscillator is added. With the use of the auxiliary oscillator a 2:1 ratio is achieved. In this configuration another interesting non linear phenomenon is observed. When the cantilever is excited at its second resonance frequency it is found that the saturation phenomena can occur. This means that when the excitation amplitude is too high at this frequency, the response of the second mode 'saturates'. The amplitude of the second mode does not increase after a critical excitation amplitude. When the second mode is 'saturated' the energy 'spills' into the first mode, and this mode activates [25].

2

2.4 Results

Table 2.1: Results for all experimental harvesters

Classification	3dB up [Hz]	3dB down [Hz]	SFoM [%]	FoMBW [-]	PNMA [1/s]	Mass [g]	Acceleration [g]
Cantilever + Magnets							
Xiong2018 [25]	3	1.5	-32.4%	0.12	3.5×10^{-6}	45	0.2
Xiong2016* [24]	1.5	3.2	-43.5%	0.11	9.4×10^{-6}	45	0.2
Two Beams and Magnets							
Wu2018 [16]	3.3	4.5	110.1%	0.19	1.3×10^{-6}	231	1.02
Yang2017*[23]	3.2	3.2	1.88%	0.14	1.5×10^{-6}	8.3	0.3
L-Shape							
Wei2018 [20]	3	-	-	0.14	5.8×10^{-6}	166.0	0.7
Nie2016*[21]	1	-	-	0.12	2.2×10^{-6}	111.3	0.2
L-Shape + Magnets							
Chen2016*[26]	3	2.5	- 10%	0.43	4.1×10^{-5}	24.4	0.05
T-Shape							
Xie2019*[27]	1.2	0.8	17.4 %	0.13	2.0×10^{-7}	92.1	0.41
T-Shape + Magnets							
Yang2018*[22]	4.5	-	-	0.19	6.2×10^{-7}	6.7	0.5

The comparisons are made to evaluate the differences between the different VEH's. There is a small dataset found that deliver the necessary information to calculate the relevant figures, these are shown in Table 2. It has to be noted that three papers did not experimentally do a frequency up- and down-sweep. The dimensionless bandwidth, PNMA and performance between up and down sweep are plotted in Fig. 2.3. Only one generator is taken from each category. The categories where there are multiple harvesters are similar and thus a similar outcome would have obtained. Except the 'Two beams and magnets' category show different behaviour, the harvester made by Wu et al. makes use of frequency up conversion [16]. This VEH is therefore not used in Fig. 2.3 but will be discussed. The abbreviations in the plots are based on the categories, so C+M is cantilever with magnets, T is the T-shape et cetera. The references with an asterisks are used to make the plots in Fig. 2.3.

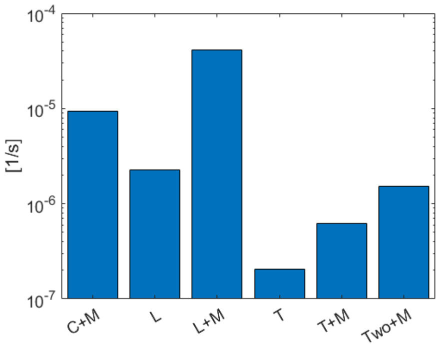

(a) Comparison PNMA

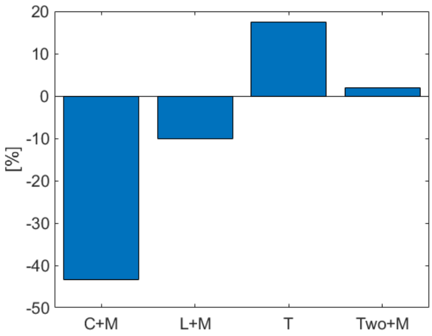

(b) Comparison performance up vs down sweeps

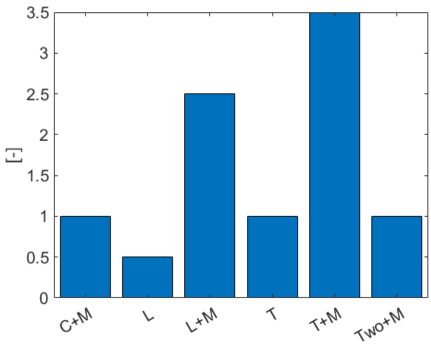

(c) Comparion Dimensionless bandwidth

Figure 2.3: Plots to compare the VEH's

2.5 Discussion

Not enough papers with experimental data have been found to make real distinctions between the different concept of internal resonance VEH's. Nothing conclusive can be said about the different concepts. However, certain trends can be seen from the data acquired and will be discussed.

From Fig. 2.3b it can be seen that different types of internal resonance VEH's have different characteristics. Different concepts show different dependence on the direction of the sweep. A noteworthy mention is the VEH made by Wu et al. [16]. They propose a frequency up-converting energy system based on internal resonance. This is done by having two beams: one assisting beam and one generating beam, both have magnets attached to them. If the assisting beam is excited at its resonance, internal resonance(3:1) will occur and the generating beam will vibrate. Because of that the generating voltage frequency is three times increased. Frequency up conversion is normally contact based, in this manner the interaction between the magnets causes the up conversion. Thus, no contact between different parts is needed. But the characteristics this system has are found to be unique out of the papers that are reviewed. This VEH has a better better 3 dB bandwidth on the down-sweep, but can generate more power in a up-sweep.

Another interesting application of internal resonance is shown by Xu et al. [28]. A multi-directional energy harvester is made using internal resonance. The design consists of a piezoelectric cantilever with a pendulum attached. Normally a piezoelectric cantilever harvester will bend due to excitations at the base of the cantilever. Xu proposes that the pendulum motion can induce bending in the cantilever beam. With the theory behind it being that internal resonance can non-linearly couple the bending mode of the beam and the swinging motion of the pendulum. Experimentally they found that the pendulum motion can indeed cause the beam to vibrate and thus harvest energy in multiple directions. Xu and Wu demonstrated that the energy pump between two modes can benefit energy harvesting besides bandwidth improvement.

It is apparent that the cantilever + magnet concept generally is able to perform better on a down-sweep than on a up-sweep. This can definitely be a deciding factor when choosing a VEH for a certain application, for example in a car as previously mentioned in section 2.2. This behaviour is due to the fact that this type of VEH has a relatively large softening nonlinearity. However, the other principles do not show such strong frequency sweep direction dependant behaviour.

When comparing the FoMBW the differences are at maximum a factor seven. The L-Shape and T-Shape with magnets seem to be the most promising in this regard. Whilst the other categories have similar FoMBW. The PNMA of the L-Shape with magnets seems to be outperforming other categories by a good margin, a drawback of this concept is mainly the volume it takes. In this review volume is not accounted for since it is not reported consistently in papers. So even though the numbers of this concept seems to be encouraging, it is offset due to the fact volume is not accounted for.

2.5.1 Future work

Out of all the categories mentioned in section 2.2 there is one where only analytical and numerical analysis have been done. No articles are found on internal resonance in buckled beams for energy harvesting where experimental work has been done. Xiong et al. [29] and Jiang et al. [30] both published articles on this subject. Both works predict bandwidth improvement and better power output when the VEH is subjected to random excitations in comparison to the linear counterpart. Nayfeh and Emam [15] have done analysis on 1:1 and 3:1 internal resonances in buckled beams. A buckled beam is compact in volume and might be an interesting topic for further research.

2.6 Conclusion

Over time VEH's are able to produce more power, but this did not enable them to be introduced in the real world. For that reason more research is being done to widen the bandwidth of the VEH. Nonlinearities can aid in this endeavour and in this review a overview is given on VEH's utilising internal resonance. It is shown from different literature that internal resonance can improve the bandwidth of VEH's due to the changing nonlinear characteristics which causes double-bending peaks in the frequency-amplitude plots. An overview is made and the different internal resonance VEH's are categorised. There are categories that show interesting behaviour when internal resonance occurs. Chaotic motion and the saturation phenomena are two examples of the rich dynamics these mechanisms can have. Internal resonance opens up new possibilities not only due to the fact that the frequency response changes. The mode coupling can also be used to enable multi-directional harvesting and frequency-up conversion. The characteristics of each category is assessed by the use of performance figures. It is shown that certain categories have large differences in the up- and down-sweep. Because of this certain internal resonance VEH's fit a certain excitation better than others. Also it has been found that buckled beams can have internal resonance, but no experimental work in energy harvesting has been done.

3

Research hypothesis

In this chapter the research hypothesis is formulated. The hypothesis is build on the found results from the literature review. From the review it became apparent that post-buckled beams can be interesting for energy harvesting. The problem with these type of harvesters is explained and a solution is proposed. This leads to the hypothesis and to validate the hypothesis models and experiments are needed. The required models and experimental testing that are needed to validate are summarised.

3.1 Post-buckled beams

It became apparent the literature review that post-buckled beams can theoretically exhibit internal resonance. However, no experimental work in energy harvesting is done to confirm the benefits of bandwidth improvement. Jiang et al. propose post-buckled beam where internal resonance is induced with intrawell motion [30]. But a different approach to the post-buckled beam is made by Ando and Cottone [31, 32]. They propose to utilise the post-buckled beam only with interwell motion, meaning that the post-buckled beam jumps between the two stable equilibria. This also leads to a bandwidth improvement since the jumping between the stable positions can happen at different frequencies, as long as the excitation amplitude is high enough. Internal resonance requires different parameters to be finely tuned for the bandwidth widening effect to work [11]. When using the interwell motion of post-buckled beams, less fine tuning is needed to see bandwidth improvement. This makes the vibration energy harvester more robust and reliable to ensure high power output along different frequencies. Therefore further research is done in this direction.

3.2 Buckling

Interwell motion in a bistable mechanism means that the mechanism jumps from one stable position to the other stable position. To be able to achieve this, an high enough input force is needed. If the input force is too low, the bistable mechanism will spring back into the stable position where it already was. A mechanism that exhibits this behaviour is a post-buckled beam. A beam is clamped on both sides, and on one side a displacement is given. This will cause the beam to buckle and this is illustrated in Fig. 3.1. This transverse displacement is described by the first buckling mode. If the beam is displaced further, the beam will exhibit a different transverse displacement. This displacement field is described by the second buckling mode [33]. Each buckling mode, has a corresponding buckling load. This load is the minimum force that needs to be applied at the end of the beam to see that specific buckling mode. These loads are denoted as $P_{crit,i}$ where i is the corresponding buckling load.

In Fig. 3.1c the interwell motion is portrayed. The beam is buckled and on the interface shown in Fig. 3.2c, a force is applied. If the force is large enough, the beam will jump to the other stable position. But during this *interwell motion*, a new displacement field is found. In this position the transverse displacement is described by the second buckling mode [34].

3.2.1 Stability and interwell motion

The stability of the equilibrium is determined by the potential energy in the mechanism. In a post-buckled beam the potential energy is stored in the form of strain energy. There are three equilibrium positions, two stable and one unstable equilibrium. In the first buckling mode the strain energy is lower than the second buckling mode. Therefore the first buckling mode is a stable position. This is because a system will always prefer to be in a lower energy state [35]. This is illustrated in Fig. 3.2a. In this illustration a ball is used. If the ball is in a stable position, the ball needs the be pushed up a hill to get to the other stable position. This is done by using an input force at the interface of the beam. The

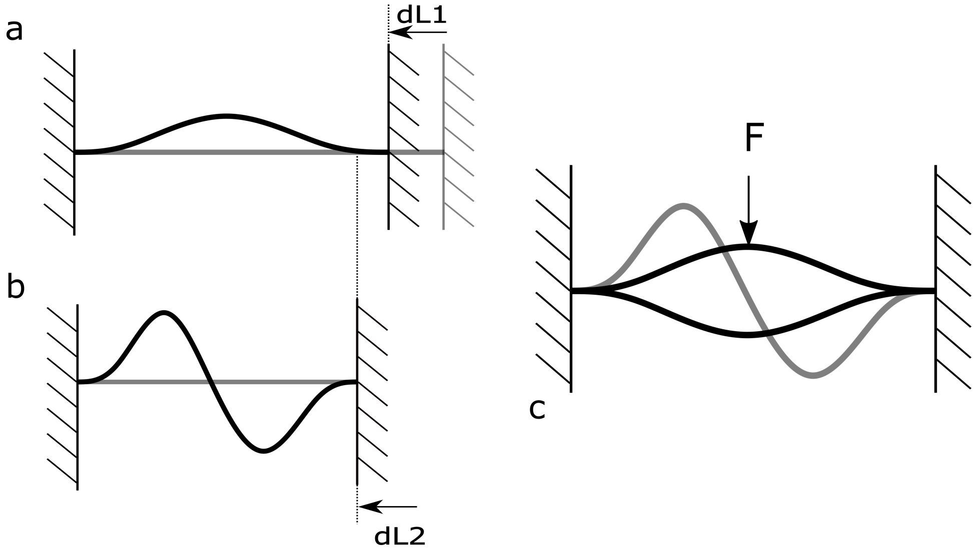

Figure 3.1: a) Beam clamped on both sides. Applying displacement dL on one side will buckle the beam. The transverse displacement is described by the first buckling mode b) Displacing further will cause the beam to buckle in its second mode shape c) Transition from upright position to downward position. Between the transition the second mode shape is observed.

height of the hill is dependent on the strain energy of the second buckling mode. If the ball is exactly on top of the hill, a small tap on the ball will cause the ball to fall in either of the two valleys. Therefore, this position is called an *unstable* equilibrium. If the ball is in the middle of the hill, the ball will always fall back in the valley, the valley is therefore a *stable* equilibrium.

So to achieve the interwell motion which is desired for energy harvesting, the potential barrier has to be surpassed. The input vibrations have to be of a large amplitude to overcome the potential barrier. In practice this is difficult because the vibrations do not have enough force to overcome this. To resolve this the barrier needs to be lowered. However, it is not practical to experimentally measure strain energy of a post-buckled beam in one of its buckling modes. This would be a direct way to measure the potential barrier and use this measurement to test the hypothesis. Another more practical approach is to measure the force-deflection characteristics of the post-buckled beam. By gradually pushing the beam from the upright position to the downward position, the force-deflection characteristics can be obtained. This characteristic is directly linked to the potential barrier of the post-buckled beam. Since the force moves along a straight path where the displacement is known the relationship between the two characteristics can be mathematically calculated. The relationship governing the force-deflection and potential barrier is $W = \int_a^b \mathbf{F}(\mathbf{s}) \cdot d\mathbf{s}$ where a and b are the initial and end coordinate respectively. The difference between a and b is then the distance travelled. Taking the derivative of the potential energy with respect to the displacement will result in the force-deflection characteristic. The slope of the force-deflection represents the stiffness of the mechanism. In 3.2 it is illustrated how

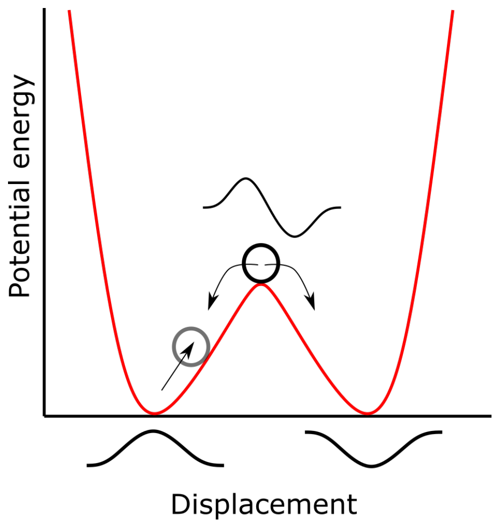

(a) Potential curves of interwell motion. Showing the stability of the equilibrium points.

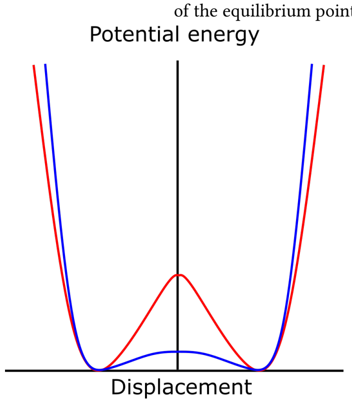

(b) Two different mechanisms comparing the potential energy vs displacement

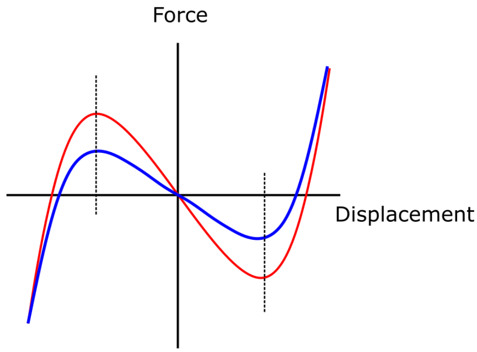

(c) Force deflections vs displacement of the two different mechanisms. Lowering the barrier reduces the stiffness. Dotted lines indicating switching points.

Figure 3.2: Potential energy and force deflection relationship

a change in the potential barrier will influence the force-deflection. The force-deflection characteristics is also more useful in energy harvesting. The force-deflection reveals the minimum force that is needed for the snap-through motion to occur. This is known as the limit or switching points and is indicated in Fig. 3.2c by the dotted lines [36]. A mass can be added in the middle of the post-buckled beam so that the snap-through motion will be easier to achieve [37]. If the mass and force are known, using Newton's second law, $F = ma$, the minimum acceleration needed from the incoming vibration can be calculated.

3.2.2 Buckling mode interaction

An interesting interaction is found by Blad et al. They propose that the difference between the first two buckling loads can be tuned to influence force-deflection behaviour. The tuning is done using shape optimizing of three predefined designs where the stiffness is locally changed. They introduced a new design parameter critical load ratio (CLR) which is defined as:

$$CLR = \frac{P_{\text{crit, 1}}}{P_{\text{crit, 2}}} \tag{3.1}$$

A uniform post-buckled beam has a CLR of 0.49 regardless of the geometry. Increasing the CLR will reduce the stiffness, this is called *buckling mode interaction* [38]. Not only the ratio is important, but also the absolute variation between the two critical buckling loads. Meaning the closer the two critical buckling loads are to each other, the more the stiffness is reduced. If they are equal (a CLR of 1) then the mechanism is statically balanced. A major benefit of this approach is that the computational cost of buckling loads is, compared to doing a force-deflection simulation or computing the strain energy in a buckling mode. This allows for more advanced tuning methods than previously performed.

3.3 Hypothesis

It has been shown that is it possible to increase the CLR of a post-buckled beam by optimizing three different predefined designs [38]. This will therefore reduce the stiffness of the post-buckled beam due to the increase of the CLR. However, no clear reason or method is given why this is the case. Removing material is a technique that can be used to tune the CLR.

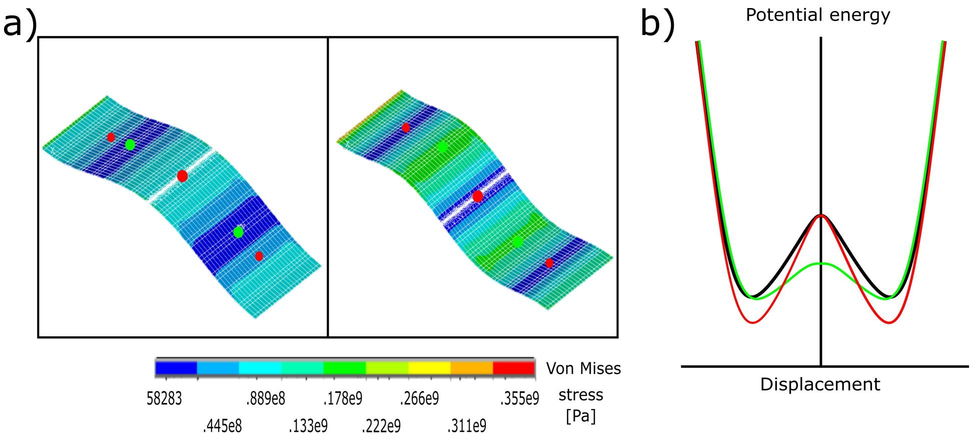

Figure 3.3: a) Left: stresses in the slender beam in the first buckling mode. Right: stresses in the slender beam in the second buckling mode. Removing material in the vicinity of the red dot will decrease buckling load two and thus decrease the stiffness. Removing material in the vicinity of the green dot will decrease buckling load one and thus increase the stiffness. b) Removing material at the location of the dots will change the potential energy curve to their respective colours. In black the potential energy curve for a homogenous beam.

In Fig. 3.3 numerical Von Mises stress simulations are shown. This simulation shows that there are parts where the stress is (close to) zero. It has to be noted that the parts where the stress is (close to) zero in the first buckling mode, differs from the parts where the stress is (close to) zero in the second buckling mode.

Strain energy is directly related to stress. If there is for example no stress in a particular area of the slender beam in the first buckling mode, then it cannot contribute to the total strain energy in that buckling mode. However, if the same area does have stress in the second buckling mode, it does contribute to the total strain energy in the second buckling mode. So when this particular area is removed it is expected that the second critical buckling load and total strain energy in this mode will lower. But the first buckling load and total strain energy in this mode should remain the same. This will bring the two buckling loads closer together and therefore lower the stiffness.

Using this logic and the numerical and the numerical results from Fig. 3.3 it seems that the opposite should also be possible. If an area is removed where the stress is zero in the second buckling mode, removing this area should not affect the second buckling load. But this area does has stress in the first buckling load, therefore removing this area should lower the first buckling load. This will increase the potential energy barrier and this is is shown in Fig. 3.3b by the red potential curve. The potential energy in buckling mode one is lowered in this scenario, therefore lowering the valley. This will cause the post-buckled beam to be stiffer. The stiffness of the beam can also be lowered by reducing the 'hill' shown in Fig. 3.3b. Lowering the 'hill' will make it easier for the interwell motion to occur. The hypothesis in this thesis is than as follows:

'Target reducing buckling loads is possible which allows to decrease and increase the stiffness in a post-buckled beam'.

To confirm this hypothesis the post-buckled beam is modelled using finite elements. The finite element model is used to simulate force-deflection behaviour and to utilise in a topology optimization.

3.4 Topology optimization

Topology optimization is a powerful tool that can be utilised to perform the tuning of the buckling loads. In topology optimization a given design space is given with boundary conditions and/or specific loads. Within this design space mathematical analysis is performed to find the best design. This differs from other optimization methods such as shape optimization, because the design can have any shape and is not predefined [39] . This method can therefore give more insight in the CLR tuning than the shape optimization previously used.

Using ANSYS Mechanical APDL as the choice of the finite element modelling package actually makes topology optimization difficult. However, we have to use this package simply because it is the best package to model the snap-through behaviour of the post-buckled beam [38]. To use this powerful finite element package a certain approach is chosen to perform the topology optimization. This differs from the norm because no gradient based algorithm is used to perform the optimization [40]. This approach was deemed the most feasible to implement and still get the desired results.

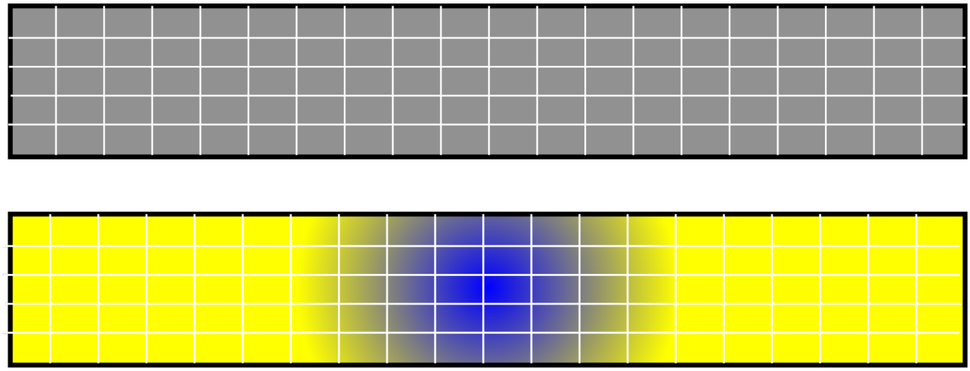

Figure 3.4: Slender beam divided in a grid. Each piece is removed to calculate the influence on the buckling loads. This can than be used to plot a colormap which will reveal. In this example the blue areas are beneficial to remove material for the objective.

3.4.1 Implementation of the topology optimization

A slender beam is divided in a grid as shown in Fig. 3.4. A piece of the grid is removed, than the buckling loads are calculated. The piece that was removed is put back, and the next piece is removed and the buckling loads are calculated. This is done for all the pieces and in this manner the influence of each piece on the buckling loads can be evaluated. The values of the buckling loads can than be put in a colormap, revealing the best locations to remove material for the objective. The same procedure can be used to either increase or decrease the stiffness.

The four best pieces are identified, because of symmetry these pieces are mirrored along the axis of the beam. When the four pieces are removed, a new colormap is generated which includes the four pieces that are already removed. This is done so the next four pieces can be identified to get closer to an optimum. This has to be done in an iterative manner because removing material at a place changes the stress distribution and therefore the strain energy in each piece.

This is al done using ANSYS Mechanical APDL. But is operated from MATLAB to perform the topology optimization. APDL needs commands to tell the program what needs to be done. A textfile is generated using MATLAB, in this file all the necessary commands are written. APDL then performs the commands and saves the results for the colormap. The process is terminated when no more improvements towards the objective can be made. In Appendix A a more detailed description of the build software is given.

4

Manipulating the stiffness of post-buckled beams using topology optimization

In this chapter the resulting article from the research is presented. In this article the hypothesis is tested with the use of analytical modelling and finite element modelling. The results from the models are experimentally verified.

4.1 Introduction

Compliant mechanisms use the flexibility of their members to acquire their motion. The advantages are their high precision for positioning, low weight and low friction [41]. A disadvantage however is that potential energy is saved in their members as strain energy. This challenges energy efficiency and disturbs the output motion of the mechanism. To compensate a negative stiffness element can be added to counteract the positive stiffness. This is called stiffness compensation [42]. A statically balanced mechanism is a system that has constant potential energy along its range of motion. This causes the mechanism to be continuously in equilibrium, resulting in motion where no force is required [43].

Bilancia et al. [44] made a zero-torque compliant mechanism by employing post-buckled beams. The post-buckled beams add negative stiffness to compensate for the positive stiffness. They achieved zero-torque within a range of 0.7 rad. A new method of statically balancing is proposed by Kuppens et al. [45] where they propose to achieve static balancing by matching the first two critical buckling loads of a mechanism. They build a MEMS device where the preloading is obtained from thermal oxidation of silicon. The device was build and measured and they showed a stiffness reduction of a factor 9 to 46. Blad et al. [38] uses the ratio of first two critical loads (CLR) as a parameter to minimize the change of potential energy between the two equilibrium positions of the buckled mechanism. Three different mechanisms are proposed, and geometrical properties are changed to investigate the influence on the CLR. It was shown that by maximizing the CLR, the required force is minimized . Numic et al. [46] used this method of stiffness compensation in a four-bar linkage mechanism. This mechanism consists of three rigid links connected with revolute joints. The three rigid links are supported by a revolute joint and a prismatic slider joint to apply the preload. In all the joints, torsion springs are integrated. This results in four torsion springs in the whole mechanism. It was found that the ratio between the buckling loads changes when the ratio of stiffness in the torsion springs changes. Using this they were able to find a configuration of the four torsion springs that led to a CLR of unity. This led to a statically balanced mechanism. This new method of matching the buckling loads has the benefit of using a linear analysis to predict non-linear behaviour which was not possible before.

However, the current tuning mechanisms do not give insights what the most effective way is to design a statically balanced mechanism using the method of buckling load matching. The research objective of this work is to develop a method for material removal from a slender beam that is the most effective to achieve buckling load matching. Topology optimization is used as a tuning mechanism which has the benefit of free design space, which was not used in previous research.

In section 2 a 2D analytical framework is given which predicts the effects of material removal. Also, the setup of the finite element analysis and topology optimization is shown. The experimental setup that is used to verify the numerical results is presented. In Section 3 the results are presented from the optimization process, the numerical analysis and how they compare with the experimental data. Section 4 the results are discussed, and conclusions are made in Section 5.

4.2 Method

4.2.1 Buckling of slender beam

Figure 4.1 depicts the buckling of a slender beam with length L and flexural rigidity EI. By compressing the beam with displacement dL, the beam will buckle. Axially compressing the beam is also known in literature as 'preloading' [47–49]. Applying a force axially past the critical buckling load of the beam will cause the beam to buckle. Its displacement field will be described by its first buckling mode [33]. The beam in its post-buckled state is bi-stable, the first buckling mode has a stable 'up' position and a stable 'down' position [50]. By pushing the beam with a force at its interface shown in Fig. 4.1, it's possible to switch between the stable equilibria. During this transition an unstable equilibrium is found, this displacement field is described by its second mode shape [34]. Each buckling mode has a corresponding critical buckling load. Theoretically there are infinite number of buckling modes with corresponding critical buckling loads, denoted with Pcrit,i where i is the represents the number of the critical buckling load. For a beam with uniform cross section the critical loads are given as follows [51]:

$$P_{\text{crit },1} = \frac{(2\pi)^2 EI}{L^2}, P_{\text{crit },2} = \frac{(2.85\pi)^2 EI}{L^2} \tag{4.1}$$

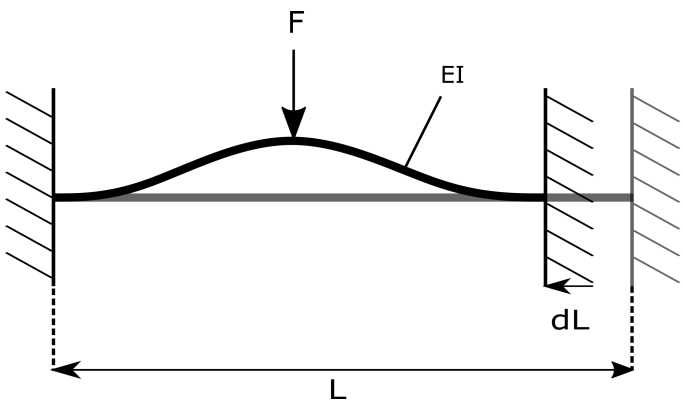

Figure 4.1: Buckling of a slender beam by applying a displacement. This causes the beam to buckle where the displacement field is described by the first buckling mode.

The distance between the first two critical buckling loads is a measure of the potential energy barrier [38]. By bringing the two critical loads closer or further this potential energy barrier decreases or increases respectively.

4.2.2 Analytical modelling

The hypothesis is that when material is removed, the critical buckling loads will lower and the magnitude of the lowering effect is determined by the magnitude of the bending moment in that piece of material. Meaning that if the bending moment is high in a piece of material in a certain buckling mode, removing that material will lower the corresponding critical load. Calculating the bending moment can be done if the displacement field is known using Euler-Bernoulli. However, the transverse displacement field of a post-buckled beam cannot be calculated analytically. Therefore, we use the mode shapes, with equations 4.3 and 4.4, the first and second mode shape can be calculated respectively.

$$P = \frac{\hat{P}\ell^2}{EI} \tag{4.2}$$

$$\psi_1(x) = c[1 - \cos(2\pi x)] \tag{4.3}$$

$$\psi_2(x) = c\left[1 - 2x - \cos\lambda x + \frac{2}{\lambda}\sin\lambda x\right] \tag{4.4}$$

$$c = \pm 2\sqrt{\frac{P}{\lambda_2^2} - 1} \tag{4.5}$$

$$\widetilde{M} = -EI\frac{d^2\widetilde{w}}{dx^2} \tag{4.6}$$

ψ_i is the mode shape where i denotes the corresponding mode; c is a constant; $\hat{P}$ is the applied axial load; P is the non dimensional load; $\lambda_2 = 8.98$ is the eigenvalue used in equations 4.4 and 4.5. Equations 4.3-4.5 are solutions to the governing buckling problem, which are given and solved by Nayfeh et. al. [52]. The bending moment in the beam can be calculated using Euler-Bernoulli in equation 4.6. Since the mode shapes that are used are not displacement fields, the bending moments obtained are not true bending moments. Therefore, the bending moment M and displacement field w are accentuated with tildes. $\widetilde{M}$ reveals where the maxima and minima bending moments are in each mode shape. The $\widetilde{M_i}$ will be scaled so that the maxima of both modes are equal to 1. This is done so that $\widetilde{M_i}$ of both modes can be visually compared. Scaling both modes to 1 makes it easier to visualize the minima/maxima and cross sections with zero as shown in Fig. 4.2c. In Fig. 4.2c it is hypothesized that the blue dots lower the first buckling load but not the second buckling load. This is because the blue dotted lines indicate that the bending moment in the first mode shape is non-zero, but in the second mode shape the bending moment is equal to zero.

4.2.3 Finite element modelling and optimization

To influence the potential barrier that is apparent when ‘snapping-through’ material will be removed. The stiffness of the beam can be determined by performing a numerical force-displacement analysis. This is done by using ANSYS Mechanical APDL using shell elements (SHELL281). In the numerical analysis the beam is gradually pushed at the interface shown in Fig. 4.1. By measuring the reaction forces and displacement in the same point, the force-deflection is determined. To avoid singularities, imperfections are induced in the beam.

A beam of 132 mm x 40 mm will be divided in a grid of 384 (16x24) pieces. An illustration is seen in Fig. 4.3. In the optimization process a new design parameter is introduced, the critical load difference (CLD). This is a variance of the CLR introduced by Blad et. al. [38] and is defined as:

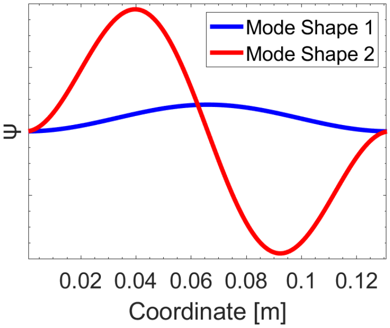

(a) Analytical mode shapes aqcuired using equations 4.3 and 4.4

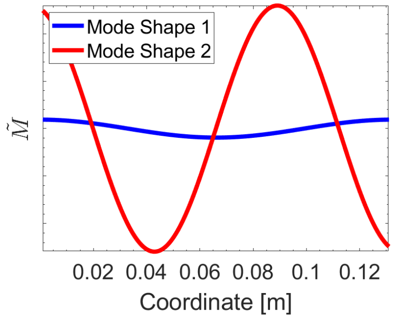

(b) Bending moment found using Euler-Bernoulli

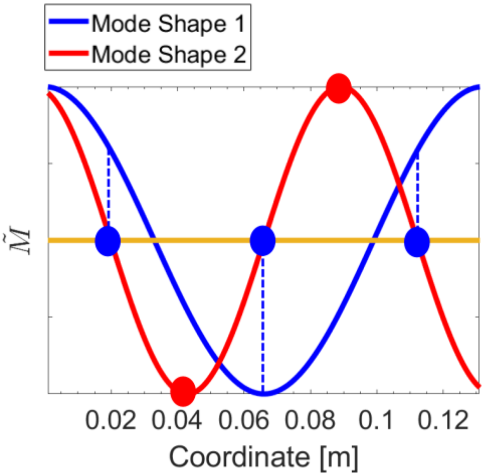

(c) Scaled bending moment where the dots indicate the area of the beam where material needs to be removed to lower a particular critical load. Blue indicating lowering the first critical buckling load and red lowering the second critical buckling load.

Figure 4.2: Results from the analytical model.

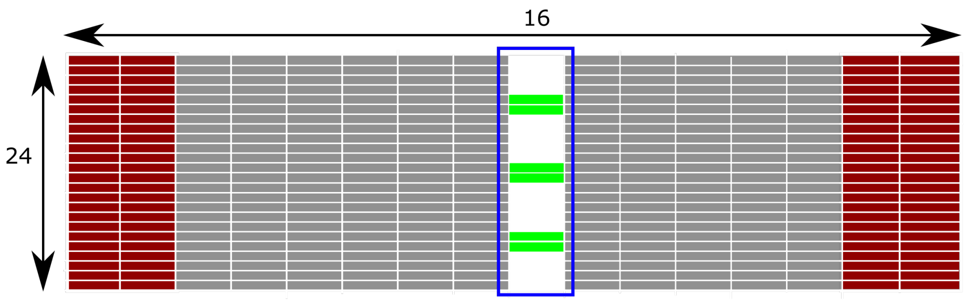

Figure 4.3: Illustration of the grid on the beam. Red marked areas are not removed. The green areas indicate the minimum width that is kept everywhere on the beam throughout the optimization process

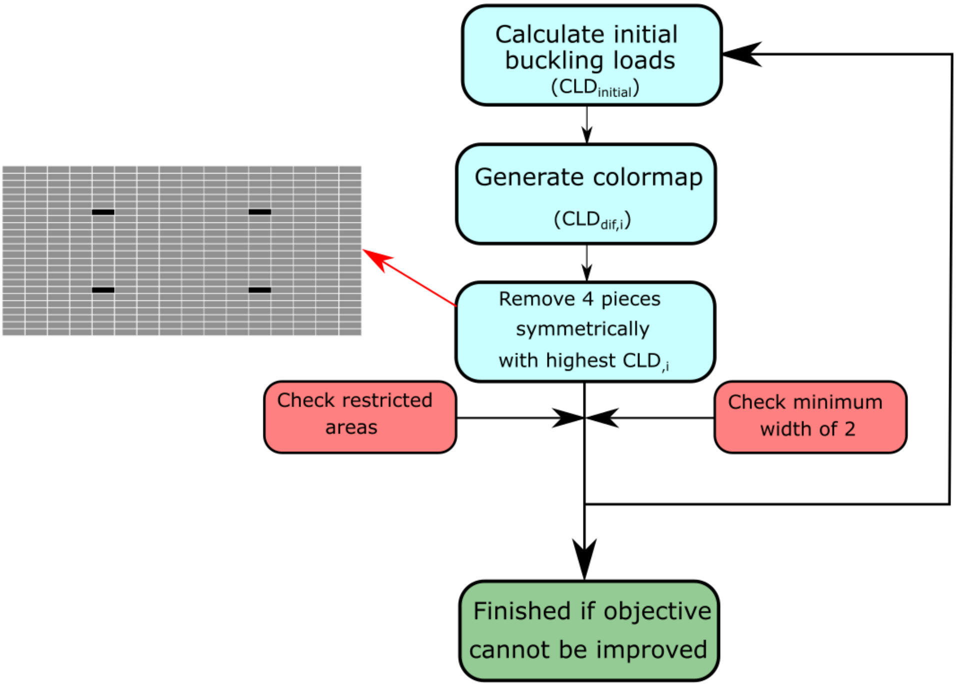

Figure 4.4: Work scheme used in the optimization process

$$CLD = P_{crit,2} - P_{crit,1} \tag{4.7}$$

The critical buckling loads of the whole beam will be calculated and the CLD is determined, and this is denoted as $CLD_{initial}$. Then a piece is removed, and the CLD is calculated and this will be denoted by $CLD_{piece,i}$, where i is the identity of the piece. To see if the critical loads come closer, the percentual change is calculated as shown in equation 4.8. This figure will be calculated for each piece of the grid and shows whether the CLD increases or decreases for that specific piece. This figure will be plotted in a colormap. This colormap will show where it is beneficial to remove material.

$$CLD_{dif,i} = \frac{CLD_{\text{piece},i} - CLD_{\text{initial}}}{CLD_{\text{initial},i}} \times 100\% \tag{4.8}$$

By removing material its is found that the buckling loads and mode shapes change. Therefore an iterative approach is chosen. The optimization is done using the following work scheme shown in Fig. 4.4.

The initial buckling loads are calculated and updated each time when material is removed. Then the buckling loads of all the pieces is calculated and the differences are determined. The constraints are checked and the piece with the highest CLD is removed and using symmetry three other pieces are also removed. The width of at minimum two pieces is for manufacturing reasons. The red marked areas are not taken into the optimization because these are necessary for clamping the slender beam. Two optimization processes will be done, one where the CLD is minimized and one where the CLD is maximized. Reducing the CLD will reduce the stiffness, whilst increasing the CLD will increase the stiffness. In Fig. 4.2c it is shown with the blue dots that when the bending moment of the second mode shape crosses zero, the bending moment in the first mode shape is non-zero. If the hypothesis is true, it would mean that removing material at the blue dots will lower the first critical buckling load, but not the second critical buckling load. Therefore it should be possible to increase the stiffness of the post-buckled beam. The predicted most effective way to reduce the second critical buckling is indicated by the red dots in Fig. 4.2c because the bending moment in the second moment is at its maximum.

4.2.4 Mechanical design

The prototypes are lasercut from 0.25 mm spring steel (E = 190 GPa). For all mechanisms the thickness,*t*, the width, *w*, the undeformed length, *L* and the axial load displacement, *dL* are the same and are shown in Table 4.1. The steel beams are put in a 3D-printed bracket. The bracket consists of two parts. The two parts have the same shape as the steel beam in its first buckled mode shape. The bracket is shorter than the undeformed length *L*. This is done to apply the axial displacement *dL*. Between these two parts the slender steel beams are placed. Then four bolts are placed in each corner through the bracket and steel beam and then fastened. By doing these the clamped boundary conditions are applied on both sides of the beam.

The force-deflection characteristics of the beams are measured using the setup shown in Figure 4.5 A FUTEK LRM200 force sensor (4) is connected to the prototype. The force sensor is then displaced using a PI M-505 motion stage (2) from which the internal encoder captures the positioning data. The data was recorded using a NI USB-6008 (1) in 200 steps of a resolution of 100 µm. The probe is fixed to the beam using a ball magnet. This magnet ensures a rolling contact and that the probe is in contact with the prototype during the whole motion. The magnet prevents the prototype to snap-through.

Table 4.1: Dimensions of the manufactured prototypes

Parameter	Symbol	Value
Length	L	132 mm
Width	w	40 mm
Axial displacement	dL	2.64 mm
Thickness	t	0.25 mm

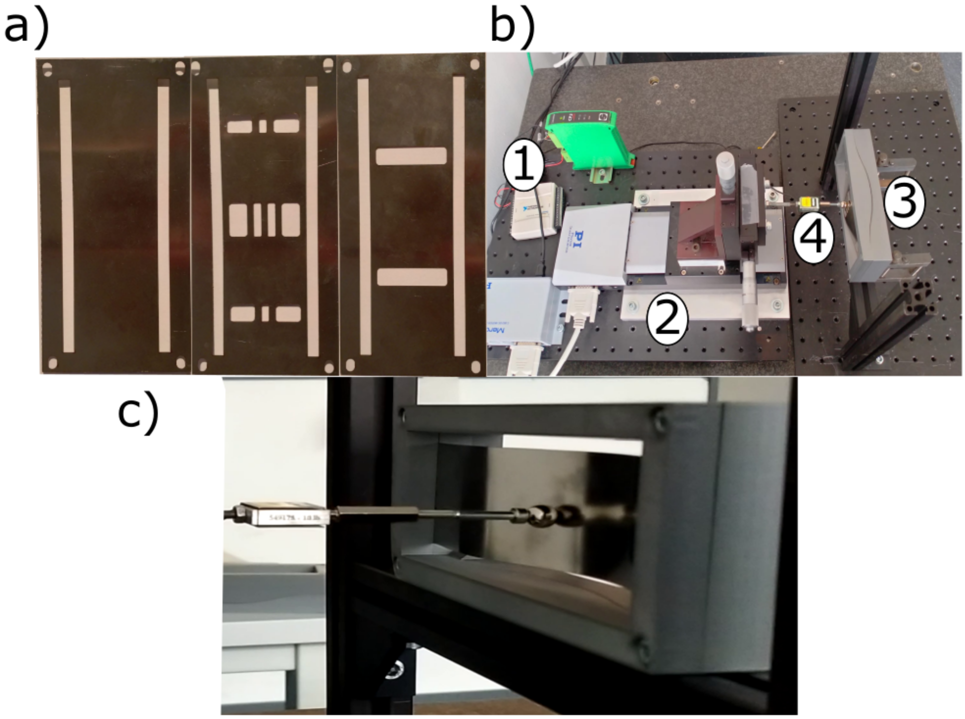

Figure 4.5: a) Manufactured mechanisms b) All the components used in the measurement c) Rolling contact using a ball magnet which ensures contact throughout the whole motion.

4.3 Results

Four iterations of the colormaps are shown. The first colormap in Fig. 4.6 indicates that to reduce the CLD, it will be the most beneficial to remove material in the dark blue areas. The second colormap in Fig. 4.6 indicates that it would be beneficial to increase this ‘slit’ along the initial blue bar. After the iterations the topology optimization is then stopped because the edges of the beam would become too small and no improvement can be made. This can be seen in the last interation in Fig. 4.6 because the beam is bright yellow, meaning that the CLD will increase.

In the next topology optimization the goal is to increase CLD, the iterations of this optimization are shown in Fig. 4.7. The colormap indicated that it the most beneficial to remove material the bright yellow areas shown in Fig. 4.7. From there material is removed so that small ‘bridges’ are formed. In the last iteration small ‘bridges’ are made at the ends of the beam. No further improvement can be made without conflicting the constraints. This beam has increased negative stiffness (INES), this abbreviation will be further used to name this beam.

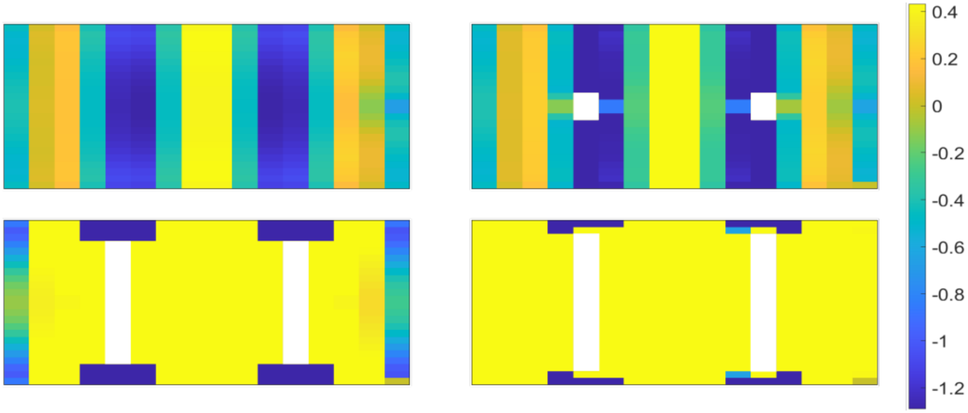

Figure 4.6: Colormaps indicating the best places to reduce the CLD shown in dark blue.

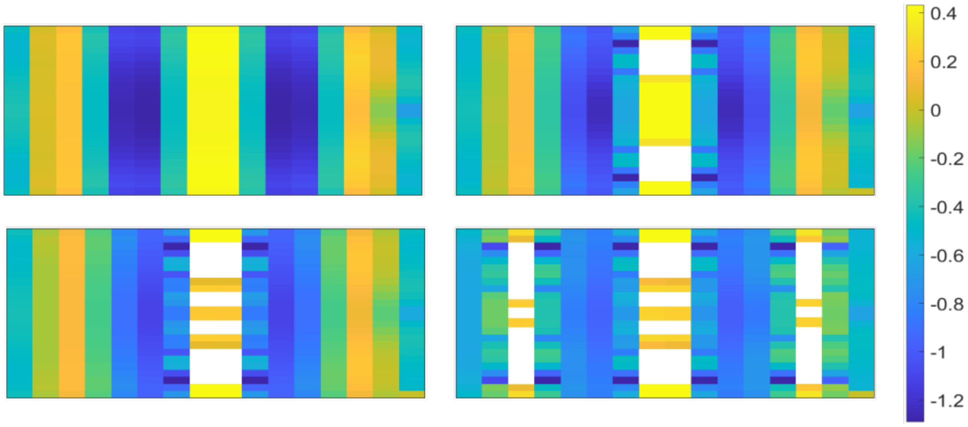

Figure 4.7: Colormaps indicating the best places to increase the CLD shown in bright yellow.

Table 4.2: Comparison between all the designs based on the finite element model for 0.25 mm beam

Mechanism	Pcrit,1 [N]	Pcrit,2 [N]	CLD [N]	Switching [N]	Stiffness change [%]	% Removed material
Whole beam	24.2	48.9	24.7	11.9	-	-
INES beam	14.3	44.0	29.3	13.5	+13.4	19
Zero beam	20.3	20.9	0.65	0.8	-93.3	10

4

(a) Whole beam : The initial beam

(b) Zero beam : Design where the CLD is minimised.

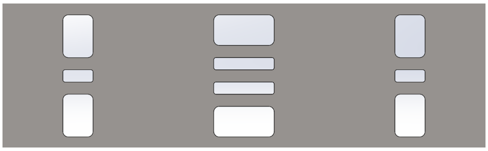

(c) INES beam : Design where the CLD is maximised.

Figure 4.8: Designs resulted from the topology optimization.

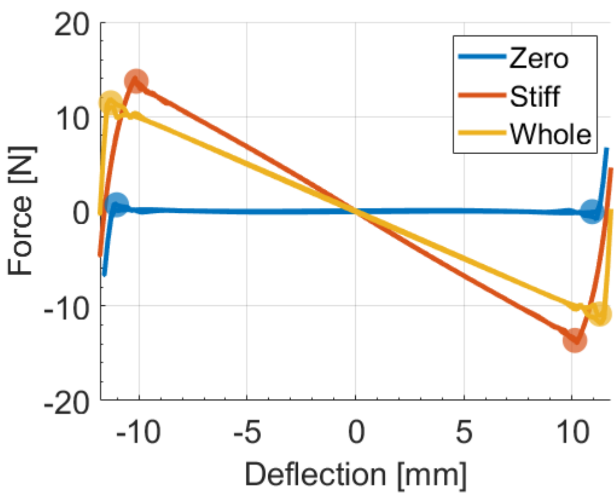

Figure 4.9: Force – deflection simulations of the different mechanisms. Transparent dots indicating the switching/limit points. The switching point for the INES beam is higher then'Whole' beam and therefore stiffer.

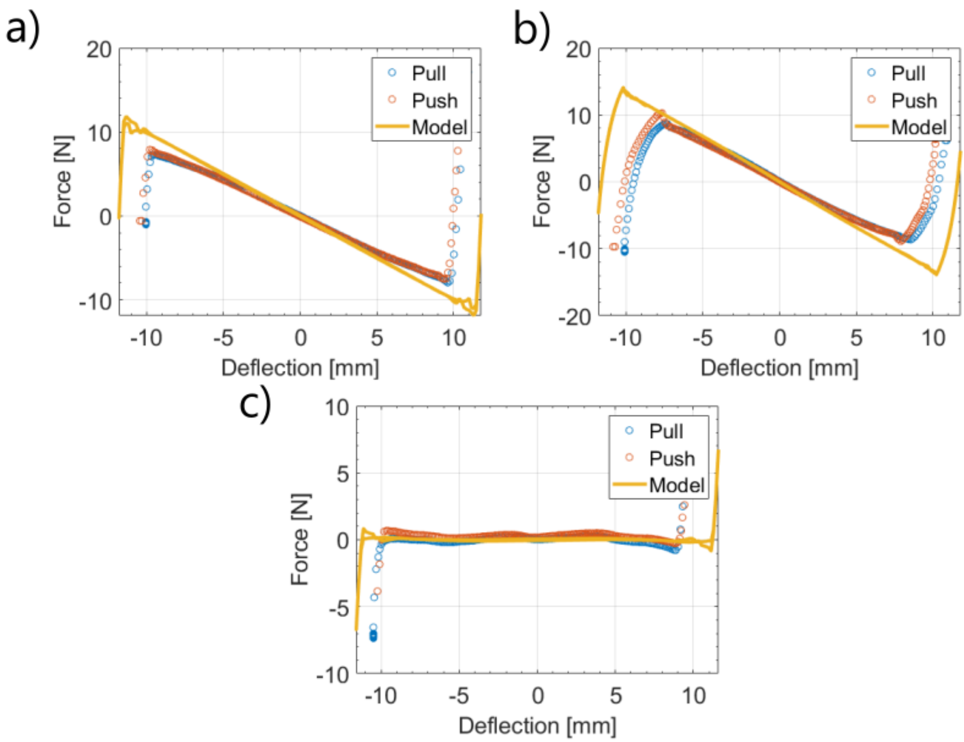

Figure 4.10: Measurement and model comparison of a) Whole beam b) INES beam c) Zero beam

4.4 Discussion

It was successful to reduce the first buckling load, whilst almost maintaining the second buckling load. This led to an increase of 4.6 N between the buckling loads in comparison with the whole beam. This is an 19% increase in the absolute difference in between the two buckling loads. This led to a significant increase in the stiffness and is shown in Fig. 4.9. The transparent dots indicating the switching/limit points are higher compared to the Whole beam. Even though 19.8% of the material is removed, a stiffer mechanism is obtained. However, the measurements verify the simulations. It can be seen in Fig. 4.9 that the INES beam is indeed stiffer than the whole beam.

4.4.1 Bending moment and the effect on lowering the buckling load

In Fig. 4.11b it can be seen that the analytical model and numerical model are in accordance. The blue dots line up with the bright yellow areas and the red dots line up with the dark blue areas. It is seen that in the ‘Zero beam’ material is removed when the function is at a maximum/minimum. When the function $\widetilde{M_2} = 0$, material is removed for the INES beam. It seems that the lowering effect of a buckling load is the most effective when a piece of material is removed with the highest bending moment in the corresponding buckling mode. Meaning that when a piece of material is removed with close to zero bending moment in its second mode shape, the second buckling load is almost not lowered. But the bending moment on this same piece of material in its first mode shape is not zero, meaning that the first buckling load will be lowered. This seems the reason why it is possible to stiffen the mechanism whilst removing material.

To show that the bending moment in a specific buckling mode determines the effectiveness of lowering the corresponding buckling load, additional colormaps are plotted. In Fig. 4.11 colormaps are shown for the individual buckling loads and overlain with the corresponding $\widetilde{M_i}$. The blue areas indicate the most effective areas to lower that specific buckling load, these areas line up with the maxima/minima of the corresponding $\widetilde{M_i}$. The yellow areas indicate the least effective areas to lower the specific buckling load, these line up with the zero cross sections of the corresponding $\widetilde{M_i}$.

The pattern that is seen in the INES beam cannot be explained by the analytical model, simply because the analytical model is in 2D. To understand the pattern, ANSYS Von Mises stresses are investigated. Two beams are compared, the original INES beam and a beam where the pattern of this beam is completely removed. Removing the pattern did not result in stiffening, meaning that the pattern is key to obtain the stiffening effect. Only one middle bridge is kept for simulation purposes.

In Fig. 4.12 the stresses in the second buckling mode of the two beams are shown. There are large areas indicated in dark blue where the stress is low, whilst in the beam with the bridges has this to a much lesser extent. The ‘bridges’ constraint this part of the beam to bend, removing these ‘bridges’ causes a large part in the beam to not bend. If this part does not bend, the potential energy decreases in this buckling mode. Therefore the bridges are necessary for the stiffening effect. In this research only the first two critical buckling loads are investigated. The same method should be able to be used to influence the CLD between higher buckling modes/loads, for example the second and third buckling mode.

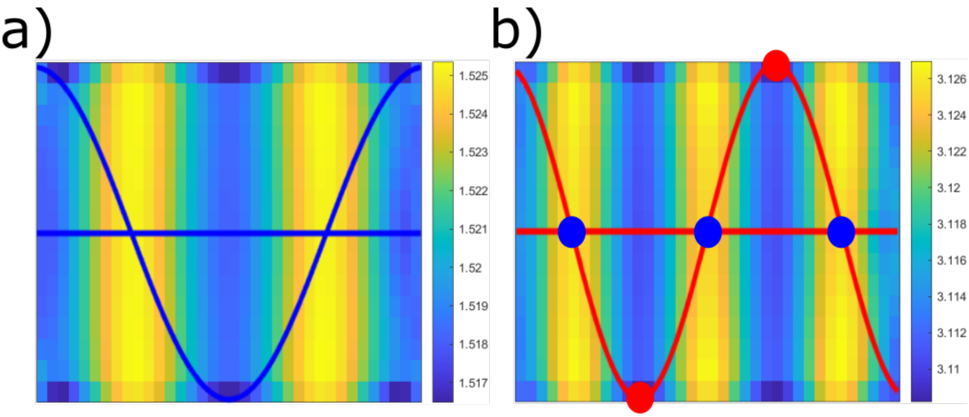

Figure 4.11: Colormaps where the individual buckling loads are plotted and overlain with their corresponding bending moment $\widetilde{M}_i$. The colormaps show in blue which areas are the most effective to reduce the buckling load. Yellow indicates negligible lowering of the buckling load. a) first buckling load b) second buckling load. The dots indicate the predicted locations of material removal shown in Fig. 4.2.

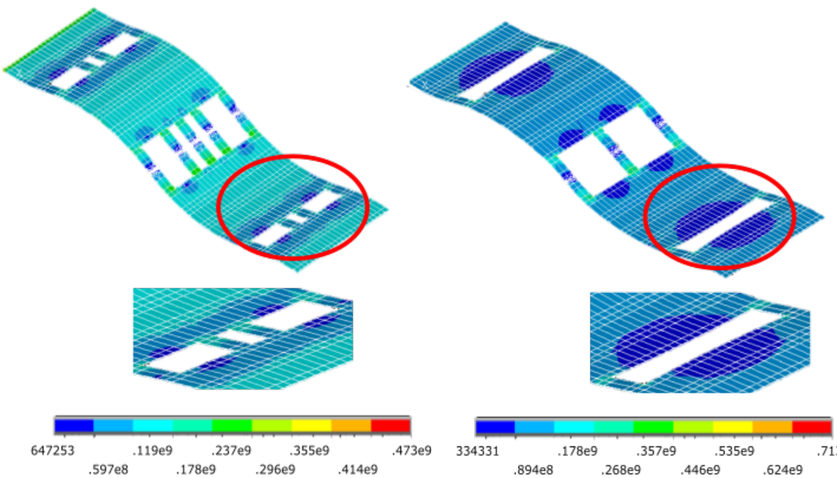

Figure 4.12: Stress comparison in first and second mode shape between INES beam and the pattern removed from the INES beam

4.4.2 Usage of the new designs

In this research it is tried to statically balance a post-buckled beam by reducing the CLD to zero. Typically another approach of statically balancing a mechanism is used, namely *stiffness compensation*. By adding a negative stiffness element to a positive stiffness so that the combination reduces the stiffness (close) to zero. The negative stiffness element can be a post-buckled beam and this already has been employed in different designs [44, 53, 54]. The negative stiffness of the post-buckled beam is dependent on its dimensions and the applied preload. With the new topologies introduced in this work another parameter is added to tune the negative stiffness of the post-buckled beam. The range of negative stiffness using this method is shown from Fig. 4.9. The negative stiffness that can be obtained can vary between the Zero stiffness beam and INES beam. Even though two designs are proposed, many more designs are possible that will have negative stiffness between this range. This became apparent from the iterative optimization process. Changing the topology of the post-buckled beam can be especially useful if the other design parameters are constraint due to the design space. Large range of negative stiffness is possible within the same design space, which was previously not possible.

Post-buckled beams have also found their use in vibration energy harvesting [31, 55, 56]. The interwell motion is desirable for vibration energy harvesting because this can improve the bandwidth of the harvester. The incoming vibrations can be too low in amplitude for the post-buckled beam to snap to its other equilibrium. The proposed methods can reduce the stiffness significantly so that interwell motion is eased and thus the bandwidth is improved. Jiao et. al. employed non-uniform post-buckled beams to improve the power output [57]. Further improvements might be obtained using the proposed designs in this work.

4.5 Conclusion

In this work buckling load tuning in post-buckled beams is optimized using topology optimization. The buckling load tuning is used to predict the force-deflection behavior of the post-buckled beam. A 2D analytical model is provided which is able to predict the locations of the minimum and maximum bending moments in each buckling mode of the beam. Removing material at locations where the bending moment is at its maximum in a buckling mode, is the most effective way to lower that respective buckling load. This is utilised to tune the buckling loads. A mechanism is obtained that is (almost) statically balanced by matching the first two buckling loads. It is also shown that it is possible to reduce the first buckling load whilst maintaining the second, resulting in a stiffer mechanism. This is verified numerically using finite-element analysis and experimentally. This stiffer mechanism is stiffer than the homogenous beam by 20%. Using the proposed methods, it is possible to significantly stiffen the post-buckled beam and get close to a statically balanced mechanism.

5
Reflection,conclusions and recommendations

In this chapter a reflection is made on the process of the graduation project. An overview is given of the different activities. Also activities that did not lead to desired results are also presented. Conclusions from the resulting research papers are done and recommendations for further research will be given.

5.1 Research activities

In Fig. 5.1 an overview is given of all the research activities that have been done during the graduation project. The graduation project spanned a time-line of 14 months, starting from September 7th 2020 to December 3th 2021. In this time the research has resulted in one paper, three prototypes and one experiment. In this graduation project a new method to manipulate the stiffness of post-buckled beams is conceived.

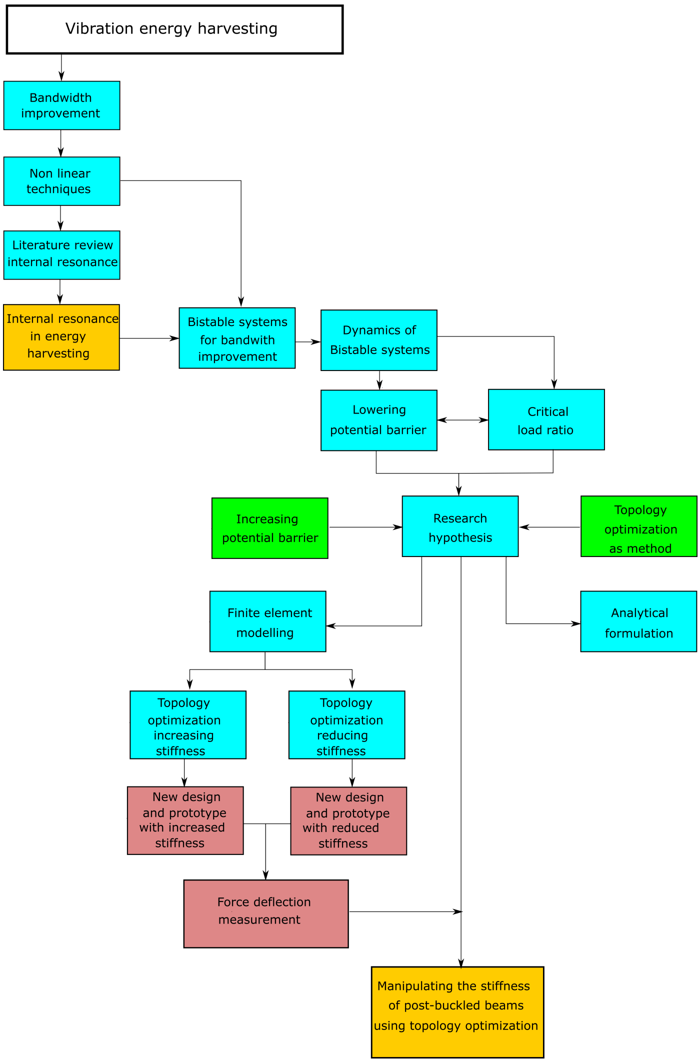

Figure 5.1: Overview of research activities. Blue blocks indicates a part of theoretical research. Red blocks indicate practical work such as experiments or manufacturing. Yellow blocks indicate research papers which resulted from the research. Green blocks indicate new ideas/concepts which are introduced in this thesis.

5.2 Reflection

The conclusions from the literature review made it appear that researching towards post-buckled beams had potential. This is because from the literature review it became apparent that internal resonance in post-buckled beams in energy harvesting has not been experimentally verified. This would seem a logical direction to do research, however it seemed difficult to achieve. Internal resonance in post-buckled beam is a highly non-linear dynamic phenomenon, making it also difficult to model analytically. This also makes it difficult to observe in practice, since certain parameters need to be well tuned before the phenomenon can occur. This requires a robust model to perform the tuning. Using different papers on dynamics of post-buckled beams it became apparent that modelling internal resonance is difficult due to the highly non linear behaviour. And frankly the lack of knowledge on the mathematical tools used to solve these type of problems made it a unfavourable direction of research. An effort was made to model this but this lead to no success. But during this the snap-through motion of a post-buckled beam was found to have potential to widen the bandwidth of energy harvesters. This led to the hypothesis that it is possible to increase and reduce to potential barrier. However, to test this hypothesis a new problem arose in finite modelling a non-uniform post-buckled beam.

5.2.1 Finite element modelling

The core of this thesis are results obtained using finite element modelling. A lot of time and effort went into understanding ANSYS Mechanical APDL. My supervisor developed a more user friendly MATLAB 'shell'. This 'shell' is a MATLAB interface that made it possible to operate ANSYS Mechanical APDL without using the complicated UI from APDL. This already made it possible to get useful results within a week. However, for my application I wanted to remove pieces of material from the beam. But the 'shell' utilised beam elements for the finite element model. This utilises one dimension geometry, making it impossible to remove material. This meant that the 'shell' that was build, needed to be adapted. This required understanding of APDL and the 'shell' that was build by my supervisor. It took around two months before any useful results could be obtained from the finite element model. But this paid of, the model is now able to quickly generate results and this allows for quickly testing new ideas.

5.2.2 Practical work

My supervisor recommended me from the start that I should not wait with using the force-deflection setup. This was based on his past experiences with experiments in general. It actually took me a while to follow this advice but in the second month I already did multiple force-deflection measurements. This was useful because I already got acquainted with the setup before doing my actual measurements. During my actual measurements I was capable to identify problems quickly. I could also verify my model that I was still building using these measurements. All the prototypes were manufactured using the laser cutter machine in IWS. This made manufacturing easy since no hands-on manufacturing was needed. Getting acquainted with the measurement setup and manufacturing beams to test in an early stage gave a head start when doing my actual measurements.

5.3 Conclusions

Vibrations energy harvesters can be utilised in many different fields, such as predicting natural disasters and supplying medical implants with electrical energy. The main problem of current vibration energy harvesters is that they are not reliable enough. Not enough power can be generated from different frequencies, the bandwidth of current harvesters is too low. Different techniques can be used to improve the bandwidth, many of them employing non linearities. In this project bi stability is used to improve the bandwidth. In order to have reliable power output for different frequencies, interwell motion is required. Being able to have continuously have interwell motion is key for optimal power output. To assure this continuous interwell motion the potential barrier between the two stable equilibrium needs to be lowered.

To achieve this the buckling loads are used as design parameters, proposed by Blad [38]. They propose that the stiffness can be lowered of a post-buckled beam by matching the first two critical buckling loads. The stiffness of a post-buckled beam is in this scenario evaluated by applying a force transversally. The reaction forces are recorded during the displacement between the two stable equilibrium. Since the distance between the buckling loads are indicators of the potential barrier, it should be possible to target reduce a buckling. Removing a piece of material that has a bending moment in the second buckling mode, but not in the first buckling mode, should only reduce the the second buckling load. Vice versa should also be true which allows reducing and increasing stiffness. This leads to the following hypothesis : *'Target reducing buckling loads is possible which allows to decrease and increase the stiffness in a post-buckled beam'*. To confirm this hypothesis a topology optimization is done using the CLD as the objective. The topology optimization is done to increase and reduce the CLD. This resulted in two different designs, one with low stiffness and one with increased stiffness compared to the uniform beam. Using numerical simulations and was experimental measurements the hypothesis was confirmed. This shows that the use of buckling loads as design parameters can be used to manipulate the stiffness in post-buckled beams. From this work it became apparent that the stiffness can be manipulated in two directions.

5.4 Recommendations

In this project the main focus was on the static characteristics of the post-buckled beam. The method can be used to improve post-buckled beams in energy harvesting by manipulating the stiffness. It is recommend to use this method to tune the post-buckled beam to the incoming vibrations. However, currently there is no method to directly link the difference between the buckling loads to the force-deflection behaviour. The current method is to try to find the desired force-deflection behaviour by trial-and-error changing the difference between the buckling loads. If these can be directly linked, the trial-and-error aspect of designing will become obsolete.

In this work two new designs are proposed using topology optimization. In this topology optimization a 24x16 grid is used, meaning that the resolution along the width of the beam was relatively high. Along the length of the beam the resolution was relatively low. Because of that the length of the holes in both new designs are suboptimal. This can be solved by using a topology optimization that is gradient based. Implementing this using

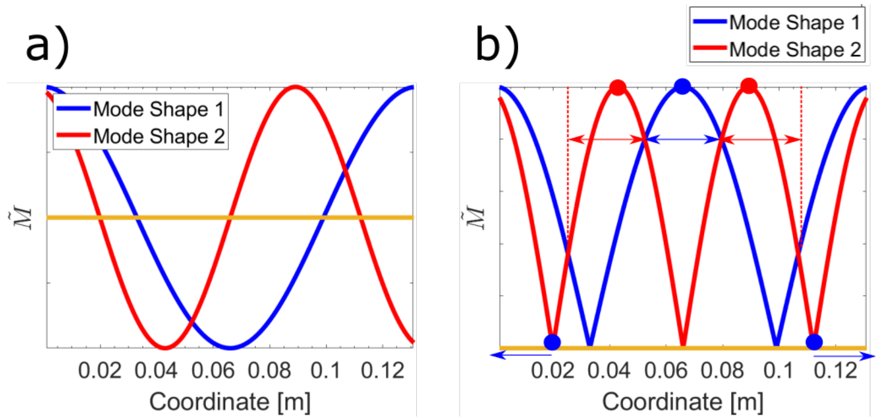

Figure 5.2: a) Bending moment of the two buckling mode scaled to 1. b) Absolute value of the bending moment scaled to 1. Dots indicating the predicted places where material needed to be removed. Red arrows showing ideal length of the holes to reduce stiffness. Blue arrows indicating ideal length of the holes to increase stiffness.

ANSYS has proven to be difficult. Another software package can be used since for the optimization process only the buckling loads are needed to be calculated. The non-linear analysis still needs to be done in ANSYS.

The length of the holes however is probably related to the cross-sections of the bending moment of the first two buckling modes. This is portrayed in Fig. 5.2. The bending moments are both scaled to one are plotted in 5.2 and the absolute values of the bending moments are plotted in 5.2b. The ideal length of the Zero beam is indicated with the red arrows and the ideal length of the INES beam is indicated with blue arrows. Blue arrows indicate where $\widetilde{M_1} > \widetilde{M_2}$ and red arrows indicate where $\widetilde{M_2} > \widetilde{M_1}$. If the real bending moments are used which can be numerically calculated, the ideal length of the holes can be determined. Note that in 5.2 the bending moments are scaled to 1 and are not representative of the real bending moments. Since the buckling modes change when material is removed, the bending moments will also change. This might also change the crossings between $\widetilde{M_1}$ and $\widetilde{M_2}$, which will change the ideal width. If this is taken into account when doing the iterative optimization process, this might lead to holes having different length further in the optimization process. This might introduce new designs that are even better than proposed in this work.

Also a dynamic model of the beam can be made, but this might prove to be difficult to do analytically because the beam is not uniform. So a numerical method is preferred, it could also simply be physically build. Using the force-deflection characteristic and the accelerations of the incoming amplitude, it can be predicted if interwell motion can occur. And to harvest energy, piezoelectric layers can be applied on the post-buckled beam. Then the power output can be measured across different incoming vibrations to establish the bandwidth of the harvester.

General advise in further research in this direction is to start building prototypes and test these in the early phase. Doing dynamic experiments in the early stages can give quicker insights in the dynamics. It also allows for quicker diagnosing of mistakes in the later stages in the research. And when a dynamic model is being build it can be compared to the measurements. Doing the experiments first gives an idea of the results that come out of the model. This can help in diagnosing mistakes in the model.

Acknowledgments

Firstly, I want to thank my supervisors Just Herder and Thijs Blad for their support throughout the project. I want to thank Thijs for the weekly meetings where tips and feedback were given. I had a difficult time in the beginning simply because I did not know which direction I should go in. But your suggestions and ideas gave me inspiration to do this graduation project, which i thoroughly enjoyed. This project was also simply not possible without the infamous MATLAPDL tool. I know you have put a lot of effort into this and I can safely say that you have single-handedly made the life of many Master students a lot easier. I want to thank Just Herder for the feedback from the session throughout the whole year. New ideas and a different point of view was definitely helpful. During the meetings you gave some out of the box ideas which inspired me to also look out of the box. The courses you gave in the first year of the Masters gave me a different way of looking at compliant mechanisms.

I also want to thank the last generation of 'stroomgraaiers' Joep, Marsha and Stijn. Due to the pandemic we only met each other physically after half a year, but the first normal weekly meeting was immediately a good laugh. The graduation phase for everyone had its ups and downs but it made it more bearable that we were all in the same boat. I could always have a chat or grab some lunch with you which made the monday actually fun. I also want to the previous generation 'stroomgraaiers'. I want to thank Armin for helping me get started with ANSYS and Joeri for helping me with my measurements.

My friends Edgar, Sacha, Tim, Tom I also want to thank you for the discussions which often were paired with drinks. Being the last of the group to graduate caused me to cancel some plans, but I will make up for it in the feature. I want to thank my cousins 'de drie wijzen uit Oost', Marlissa , Rosangela and Rowanita. Even though I am an only child, I never felt that way because of you. I always had three sisters but you were just from my second mom.

I am writing the last words of my Master thesis, which would definitely not be possible without my mom. The emotional support not only during this graduation project, but since my childhood made it possible for me to get where I am.

Rajiv
Amstelveen, November 2021

5

Appendices

A

Adapting the finite element model

A

For analysing post-buckled beams ANSYS Mechanical APDL is the chosen finite element package. The solvers of APDL offer many options to deal with buckling, post-buckling and geometric nonlinearities it is preferred over COMSOL [58]. However, the user interface (UI) of ANSYS is incredibly difficult to use. To circumvent this problem Matlab is used to control ANSYS without using the UI of ANSYS. An app was developed by Thijs Blad called *MATLAPDL Control Panel*. This app makes use of beam elements. For this research beam elements cannot be used since only 1D geometry can be used. Therefore the existing model needed to be changed. This chapter showcases the changes that needed to be made to the developed app for the analysis that have been done. For all the calculations shell elements have been used. In this graduation project this adapted tool was used to generate all the results. This app writes a script of APDL commands and this script can be executed from Matlab. Also the results are also saved and can be processed by Matlab.

To let MATLAPDL generate the correct APDL commands, it requires information about the mechanism.

- Material
- Topology
- Loads

Material

In the Material section the Young's modulus, the Poisson's ratio and density are required. In this study spring steel is used with a Young's modulus of 190 GPa, Poisson's ratio of 0.33 and a density of 7890 kg/m^3. Using the following APDL commands the material characteristics are set:

```
MPDATA,EX,1,,190000000000
MPDATA,PRXY,1,,0.34
MPDATA,DENS,1,,7890
```

Topology

For this application we divide a beam into a grid as shown in Fig. A.1. To generate this grid ANSYS uses keypoints which are shown in black dots in Fig. A.1 to build geometry.

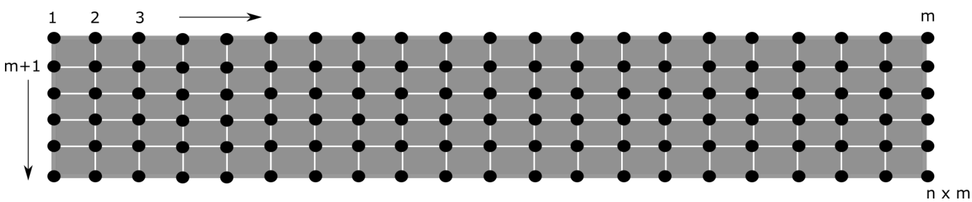

Figure A.1: Beam divided in a grid. Black dots are the keypoints.

A n x m grid is made where the counting starts at the top left corner with coordinates (0,0) and goes further in the horizontal direction. *n x m is defined as the amount of keypoints in each direction.* Knowing the length and width of the beam each coordinate can be calculated for all the keypoints. The distance between each keypoint along the length and width of the beam can than be calculated by:

$$\begin{aligned} L_{el} &= \frac{L}{m-1} \\ W_{el} &= \frac{W}{m-1} \end{aligned} \tag{A.1}$$

A vector that contains the coordinates of the grid can than be calculated by :

$$\begin{aligned} x &= \begin{bmatrix} L_{el} \cdot 0 & L_{el} \cdot 1 & L_{el} \cdot 2 & \ldots & L_{el} \cdot m \end{bmatrix} \\ z &= \begin{bmatrix} W_{el} \cdot 0 & W_{el} \cdot 1 & W_{el} \cdot 2 & \ldots & W_{el} \cdot n \end{bmatrix} \end{aligned} \tag{A.2}$$

Using the meshgrid function in Matlab the coordinates off all keypoints can be generated and are stored in a matrix. By some post-processing the keypoints can be arranged in order with their corresponding x and z coordinates. An example is shown of how this can be done:

```
% Mesh the grid given from the grid vectors
[X,Z] = meshgrid(x,z);
coords = [X(:) Z(:)];
% Y is full of zeros
null = zeros(size(coords,1),1);
% Keypoints matrix
Keypoints = [X(:) null Z(:)];
% Sort it so that the keypoints are in the right direction
Keypoints = sortrows(Keypoints,3,'descend');
```

Note that an extra column needs to be added with zeros in the Y direction since ANSYS always works in three dimensions. Now all the keypoints have been calculated and sorted. Using the MatlAPDL the commands for all the keypoints can be easily generated. An example for the keypoints APDL commands for a 25x17 grid are given:

K,1,0,0,0
K,2,0.00825,0,0
K,3,0.0165,0,0
K,4,0.02475,0,0

Now the keypoints have been defined, the areas between all the keypoints have to be defined. The area command in ANSYS requires as input four keypoints. So for the top left area shown in Fig. A.1, the command is *A , 1 , 2 , m +1 , m + 2.* The areas are numbered in ANSYS by input order, this is important for the topology optimization. Area 2 should then be *A , 2 , 3 , m +2 , m + 3*, the keypoints are counted clockwise and starts from the top left. An example of the APDL commands of a 25x17 grid is given:

A,1,2,19,18
A,2,3,20,19

A

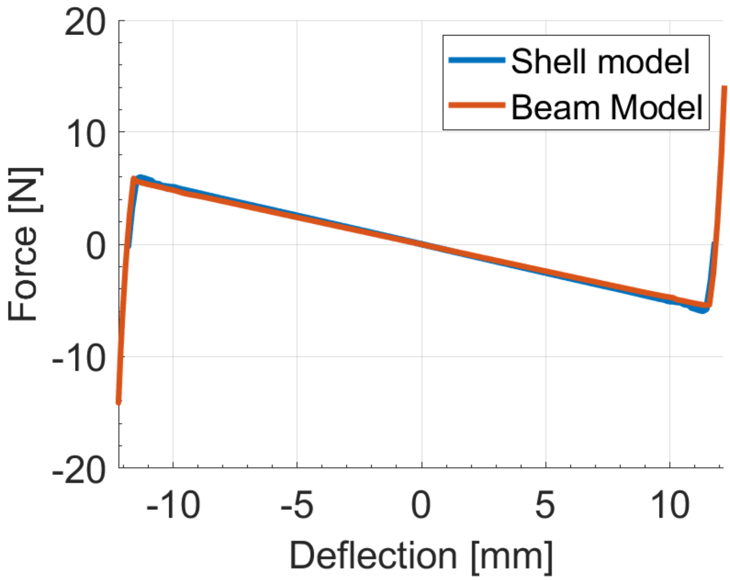

Figure A.2: Shell model versus the reference beam model. Shell model and beam model provide the same results.

```
A,3,4,21,20
A,4,5,22,21
```

Meshing

In this project the use of SHELL281 elements has been used. Other element types have been extensively tried but for the large deflections that are apparent in this application, SHELL 281 performed the best. The results of the SHELL281 have been compared to the originally used BEAM188 model. In Fig. A.2 it can be seen that the numerical results found are equal.

The element size in this project is mainly chosen by ANSYS using the Smartsizing function. Smartsize allows the user to 'refine' the mesh between a scale from 1 to 10, 1 being the finest and 10 the most coarse. Typically this gives decent results but more complex geometry might need manual intervention. The following meshing commands are used:

```
SMRT,10
MSHAPE,0,2D
MSHKEY,0
ASEL,ALL
CM,_Y1,AREA
CHKMSH,'AREA'
CMSEL,S,_Y
AMESH,_Y1
CMDELE,_Y
```

CMDELE,_Y1
CMDELE,_Y2

Boundary conditions and Loads

The beam is clamped on both sides, meaning no translations or rotations. However, a displacement is given on the right side of the beam for the preloading. In Fig. A.3 it is shown where the boundary conditions are applied. The boundary conditions are applied at the nodes of the meshed model. In order to find the nodes, APDL commands are needed to select these nodes. To do this we to do the following procedure:

- Find the keypoints indicated with green and red in Fig. A.3.
- Find the corresponding lines between the keypoints
- Find the nodes that correspond with each line and apply the boundary conditions.

The lines can be found when two keypoints are selected in ANSYS. ANSYS can select the corresponding line when two keypoints are selected. To find the keypoints in red shown in Fig. A.3, the following scheme was used:

$$\begin{aligned} kp_1 &= \begin{bmatrix} 1+m\times(1-1) & 1+m\times(2-1) & 1+m\times(3-1) & \dots & 1+m\times(n-1)-1) \end{bmatrix} \\ kp_2 &= \begin{bmatrix} 1+m\times 1 & 1+m\times 2 & 1+m\times 3 & \dots & 1+m\times(n-1) \end{bmatrix} \end{aligned} \tag{A.3}$$

To acquire the keypoints of the green dots shown in Fig. A.3, this scheme was used:

$$\begin{aligned} kp_1 &= \begin{bmatrix} m\times(1-1)+m & m\times(2-1)+m & m\times(3-1)+m & \dots & m\times(n-1)+m \end{bmatrix} \\ kp_2 &= \begin{bmatrix} m\times 1+m & m\times 2+m & m\times 3+m & \dots & m\times n+m \end{bmatrix} \end{aligned} \tag{A.4}$$

The outcome of these schemes are matrices where the keypoints are arranged so that we can find the needed lines using ANSYS commands. These lines are necessary to apply the correct boundary conditions. An example of these matrices is shown in Fig.A.4.

One boundary conditions on the left side of the beam are defined with the following ANSYS commands:

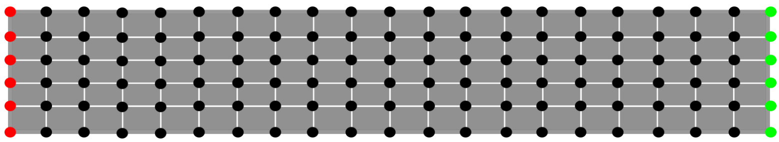

Figure A.3: Red dots indicating clamped boundary conditions. Green dots indicating clamped boundary conditions but with a displacement in the x-direction for the preloading.

```
KSEL,S, , ,1
KSEL,A, , ,18
LSLK,S,1
NSLL,S,1
D,ALL,ALL,0
```

Note that this command needs to be done for all the lines on the left side of the beam. For the right side the commands are as follows:

```
KSEL,S, , ,17
KSEL,A, , ,34
LSLK,S,1
NSLL,S,1
D,ALL,UY,0
D,ALL,UZ,0
D,ALL,ROTX,0
D,ALL,ROTY,0
D,ALL,ROTZ,0
ALLSEL
```

All the degree-of-freedom are constraint on the right side, except the displacement in the x-direction. On the right side the desired displacement can be applied so that the beam will buckle. The displacement only needs to be applied on one node on the right side.

Applying these to the existing MATLAPDL software developed by Thijs Blad enabled the ability to do the topology optimization. No adaptations are needed for the simulation of the force-deflection, the exact same commands from the BEAM188 model can be used.

	1	2
1	1	18
2	18	35
3	35	52
4	52	69
5	69	86
6	86	103
7	103	120
8	120	137

	1	2
1	17	34
2	34	51
3	51	68
4	68	85
5	85	102
6	102	119
7	119	136
8	136	153

Figure A.4: An example of the matrices produced by the schemes in equations A.3 and A.4. In each row there are two keypoints which defines a line.

B

Technical drawings of all the manufactured designs

B

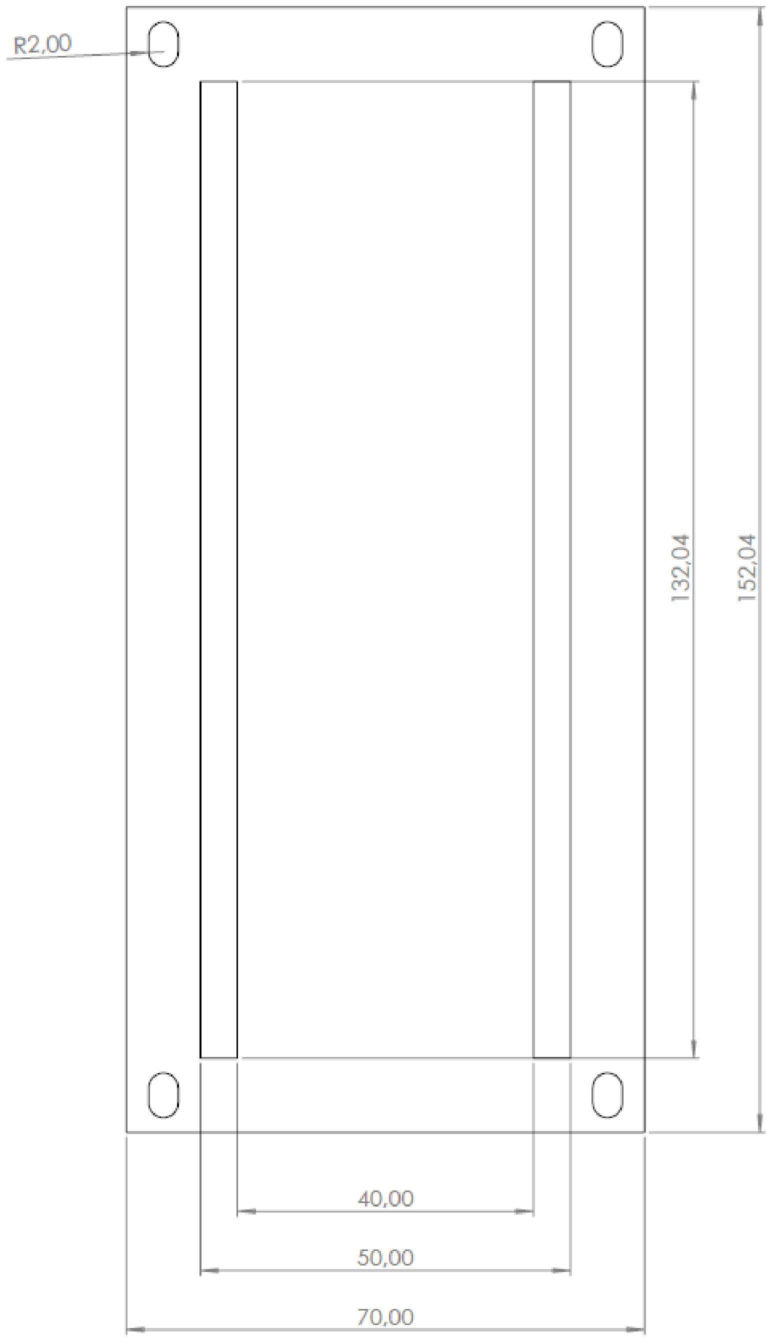

Figure B.1: Technical drawing of the Whole beam

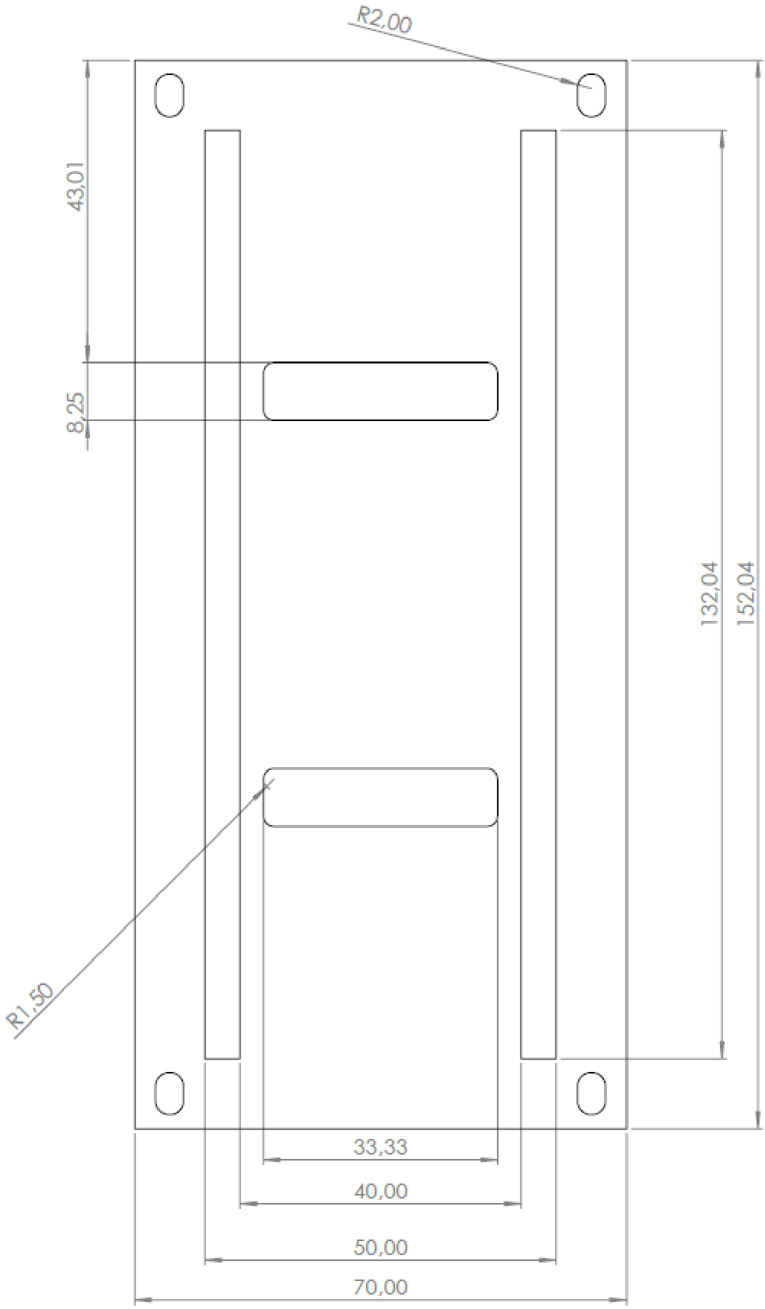

Figure B.2: Technical drawing of the Zero beam

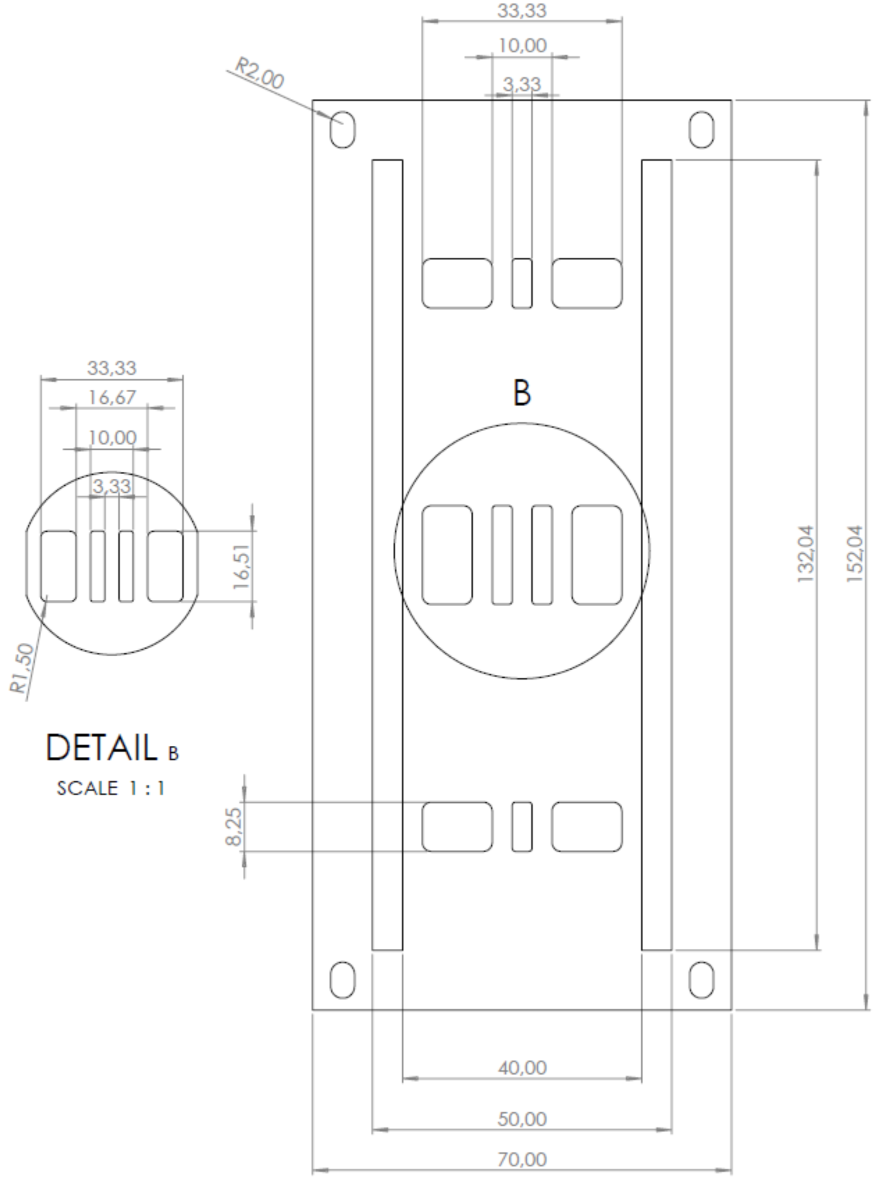

Figure B.3: Technical drawing of the INES beam

C

Refining the grid for increasing CLD

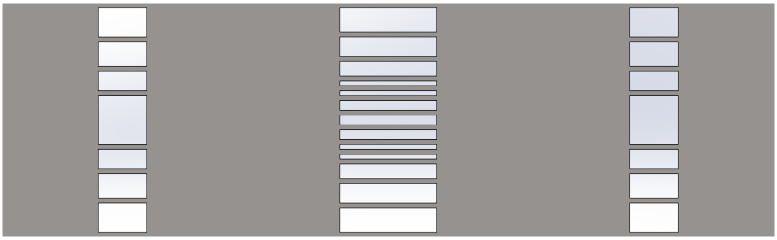

Figure C.1: Design where the CLD is increased with a finer grid. The same 'bridges' are apparent as in the INES Beam.

All the results in the thesis are gotten using a 24x16 grid. In this chapter the CLD is increased but using a 48x16 grid. This was done to see how the design would change and if the stiffness could be increased even further. This refined grid is not used in the thesis due to the computational cost. The design that was generated in Fig. C.1 took twenty hours to compute. The same work scheme in 4.4 is used for this optimization process.

Refining the grid led to a new design where the same characteristics are seen as the INES beam. In both designs the 'bridges' are apparent and the gaps on the edges of the beam are bigger than in the middle of the beam However, the new design does not improve the stiffness significantly more. The same amount of material is removed in the refined design. In terms of switching, the stiffness is not increased. This is can be seen by the transparent dots in C.2, where the switching point of the INES beam is equal to the switching point of the new design. The main difference in the static behaviour is the negative stiffness and the reduction in of range of motion. Due to the small features, this design was not manufactured.

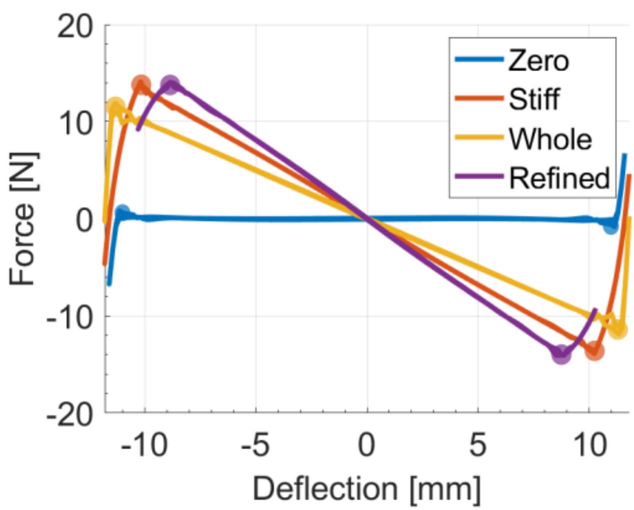

Figure C.2: Force – deflection simulations of the different mechanisms. Transparent dots indicating the switching/limit points. For the INES and 'Refined' beams these are higher than the 'Whole' beam and therefore stiffer.

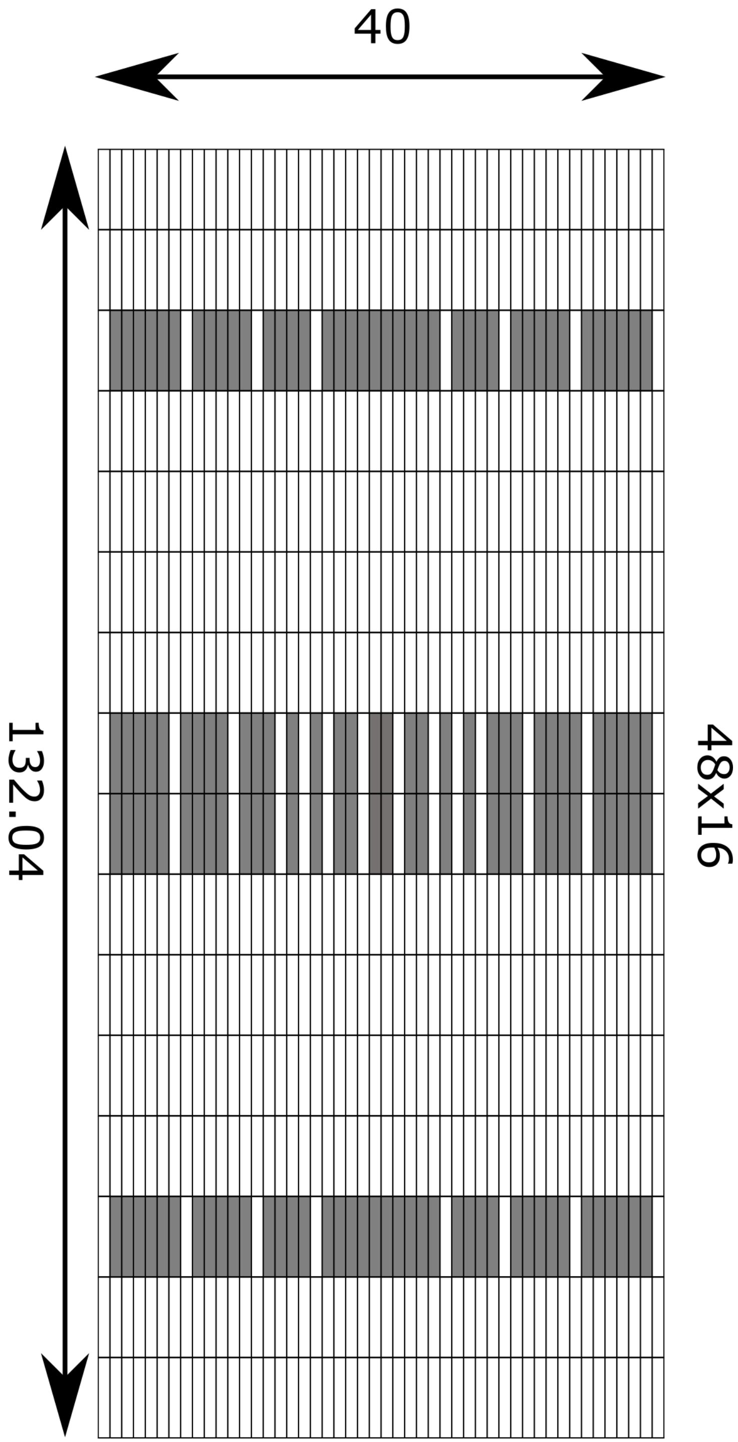

Figure C.3: Refined grid of the beam. Grey areas indicate that these pieces are removed. Using the dimensions and the grid size the dimensions of the features can be calculated.

Bibliography

References

[1] Dagobert G. Kessel. Global warming - facts, assessment, countermeasures. *Journal of Petroleum Science and Engineering*, 26(1-4):157–168, 2000.

[2] Insight: Five examples why f1 is accelerating the future.

[3] Yajuan Yu, Bo Chen, Kai Huang, Xiang Wang, and Dong Wang. Environmental impact assessment and end-of-life treatment policy analysis for Li-ion batteries and Ni-MH batteries. *International Journal of Environmental Research and Public Health*, 11(3):3185–3198, 2014.

[4] Jessy Baker, Shad Roundy, and Paul Wright. Alternative geometries for increasing power density in vibration energy scavenging for wireless sensor networks. *Collection of Technical Papers - 3rd International Energy Conversion Engineering Conference*, 2(August):959–970, 2005.

[5] Mohamed Hefeeda and Majid Bagheri. Wireless sensor networks for early detection of forest fires. *2007 IEEE Internatonal Conference on Mobile Adhoc and Sensor Systems, MASS*, (August 2003), 2007.

[6] Liyang Yu, Neng Wang, and Xiaoqiao Meng. Real-time forest fire detection with wireless sensor networks. *Proceedings - 2005 International Conference on Wireless Communications, Networking and Mobile Computing, WCNM 2005*, 2:1214–1217, 2005.

[7] Jane K. Hart and Kirk Martinez. Environmental Sensor Networks: A revolution in the earth system science? *Earth-Science Reviews*, 78(3-4):177–191, 2006.

[8] Lin Dong, Andrew B. Closson, Congran Jin, Ian Trase, Zi Chen, and John X.J. Zhang. Vibration-Energy-Harvesting System: Transduction Mechanisms, Frequency Tuning Techniques, and Biomechanical Applications. *Advanced Materials Technologies*, 4(10):1–28, 2019.

[9] T. T. Toh, S. W. Wright, and P. D. Mitcheson. Resonant frequency tuning of an industrial vibration energy harvester. *Journal of Physics: Conference Series*, 557(1), 2014.

[10] Robert Rantz and Shad Roundy. Characterization of real-world vibration sources with a view toward optimal energy harvesting architectures. *Industrial and Commercial Applications of Smart Structures Technologies 2016*, 9801:98010P, 2016.

[11] Ngan Tran, Mergen H. Ghayesh, and Maziar Arjomandi. Ambient vibration energy harvesters: A review on nonlinear techniques for performance enhancement. *International Journal of Engineering Science*, 127:162–185, 2018.

[12] D. G. Lee, G. P. Carman, D. Murphy, and C. Schulenburg. Novel micro vibration energy harvesting device using frequency up conversion. *TRANSDUCERS and EUROSENSORS '07 - 4th International Conference on Solid-State Sensors, Actuators and Microsystems*, pages 871–874, 2007.

[13] Yu Jia. Review of nonlinear vibration energy harvesting: Duffing, bistability, parametric, stochastic and others. *Journal of Intelligent Material Systems and Structures*, 31(7):921–944, 2020.

[14] Wolfgang Kliemann. *Nonlinear Dynamics and Stochastic Mechanics.* 2018.

[15] Samir A. Emam and Ali H. Nayfeh. Non-linear response of buckled beams to 1:1 and 3:1 internal resonances. *International Journal of Non-Linear Mechanics*, 52:12–25, 2013.

[16] Yipeng Wu, Hongli Ji, Jinhao Qiu, Weiqun Liu, and Jinling Zhao. An internal resonance based frequency up-converting energy harvester. *Journal of Intelligent Material Systems and Structures*, 29(13):2766–2781, 2018.

[17] A. Cammarano, S. A. Neild, S. G. Burrow, and D. J. Inman. The bandwidth of optimized nonlinear vibration-based energy harvesters. *Smart Materials and Structures*, 23(5), 2014.

[18] Paul D. Mitcheson, Eric M. Yeatman, G. Kondala Rao, Andrew S. Holmes, and Tim C. Green. Energy harvesting from human and machine motion for wireless electronic devices. *Proceedings of the IEEE*, 96(9):1457–1486, 2008.

[19] W. Q. Liu, A. Badel, F. Formosa, and Y. P. Wu. A new figure of merit for wideband vibration energy harvesters. *Smart Materials and Structures*, 24(12), 2015.

[20] Jiaying Wei, Emily Engel, and Christopher L. Lee. An Extended-Range Vibration Energy Harvester Based on Internal Resonance. *IEEE Sensors Journal*, 18(3):995–1005, 2018.

[21] Xiaochun Nie, Ting Tan, Zhimiao Yan, Zhitao Yan, and Muhammad R. Hajj. Broadband and high-efficient L-shaped piezoelectric energy harvester based on internal resonance. *International Journal of Mechanical Sciences*, 159(January):287–305, 2019.

[22] Wei Yang, Alwathiqbellah Ibrahim, and Shahrzad Towfighian. Internal resonance of T-shaped structure for energy harvesting with magnetic nonlinearity. (March 2018):85, 2018.

[23] Wei Yang and Shahrzad Towfighian. Internal resonance and low frequency vibration energy harvesting. *Smart Materials and Structures*, 26(9), 2017.

[24] Liuyang Xiong, Lihua Tang, and Brian R. Mace. Internal resonance with commensurability induced by an auxiliary oscillator for broadband energy harvesting. *Applied Physics Letters*, 108(20), 2016.

[25] Liuyang Xiong, Lihua Tang, and Brian R. Mace. A comprehensive study of 2:1 internal-resonance-based piezoelectric vibration energy harvesting. *Nonlinear Dynamics*, 91(3):1817–1834, 2018.

[26] Li Qun Chen, Wen An Jiang, Meghashyam Panyam, and Mohammed F. Daqaq. A broadband internally resonant vibratory energy harvester. *Journal of Vibration and Acoustics, Transactions of the ASME*, 138(6):1–10, 2016.

[27] Zhengqiu Xie, Tao Wang, C. A.Kitio Kwuimy, Yimin Shao, and Wenbin Huang. Design, analysis and experimental study of a T-shaped piezoelectric energy harvester with internal resonance. *Smart Materials and Structures*, 28(8), 2019.

[28] Jiawen Xu and Jiong Tang. Modeling and analysis of piezoelectric cantilever-pendulum system for multi-directional energy harvesting. *Journal of Intelligent Material Systems and Structures*, 28(3):323–338, 2017.

[29] Liuyang Xiong, Lihua Tang, Hu Ding, Liqun Chen, and Brian Mace. Broadband performance of a piezoelectric energy harvester based on the internal resonance of buckled beam. *Active and Passive Smart Structures and Integrated Systems 2016*, 9799(April 2016):97993O, 2016.

[30] Wen An Jiang, Li Qun Chen, and Hu Ding. Internal resonance in axially loaded beam energy harvesters with an oscillator to enhance the bandwidth. *Nonlinear Dynamics*, 85(4):2507–2520, 2016.

[31] B. Andò, S. Baglio, A. R. Bulsara, and V. Marletta. A bistable buckled beam based approach for vibrational energy harvesting. *Sensors and Actuators, A: Physical*, 211:153–161, 2014.

[32] F. Cottone, L. Gammaitoni, H. Vocca, M. Ferrari, and V. Ferrari. Piezoelectric buckled beams for random vibration energy harvesting. *Smart Materials and Structures*, 21(3), 2012.

[33] B. Camescasse, A. Fernandes, and J. Pouget. Bistable buckled beam and force actuation: Experimental validations. *International Journal of Solids and Structures*, 51(9):1750–1757, 2014.

[34] Jian Zhao, Nyuan Jia, Xiaoping He, and Hongxi Wang. Post-buckling and snap-through behavior of inclined slender beams. *Journal of Applied Mechanics, Transactions ASME*, 75(4):0410201–0410207, 2008.

[35] Murari Lal Gambhir. *Stability analysis and design of structures*. Springer, 2011.

[36] N A Alfutov. *Stability of elastic structures*, volume 3. 1976.

[37] A. J. Sneller, P. Cette, and B. P. Mann. Experimental investigation of a post-buckled piezoelectric beam with an attached central mass used to harvest energy. *Proceedings of the Institution of Mechanical Engineers. Part I: Journal of Systems and Control Engineering*, 225(4):497–509, 2011.

[38] T. W.A. Blad, R. A.J. van Ostayen, and N. Tolou. A method for tuning the stiffness of building blocks for statically balanced compliant ortho-planar mechanisms. *Mechanism and Machine Theory*, 162:1–11, 2021.

[39] Ole Sigmund and Kurt Maute. Topology optimization approaches: A comparative review. *Structural and Multidisciplinary Optimization*, 48(6):1031–1055, 2013.

[40] Ole Sigmund. On the usefulness of non-gradient approaches in topology optimization. *Structural and Multidisciplinary Optimization*, 43(5):589–596, 2011.

[41] Vincenzo Parenti-Castelli and Nicola Sancisi. *Synthesis of Spatial Mechanisms to Model Human Joints*. 2013.

[42] Karin Hoetmer, Just L. Herder, and Charles J. Kim. A Building Block Approach for the design of statically balanced compliant mechanisms. *Proceedings of the ASME Design Engineering Technical Conference*, 7(PARTS A AND B):313–323, 2009.

[43] Juan A. Gallego and Just Herder. Criteria for the static balancing of compliant mechanisms. *Proceedings of the ASME Design Engineering Technical Conference*, 2(PARTS A AND B):465–473, 2010.

[44] Pietro Bilancia, Samuel P. Smith, Giovanni Berselli, Spencer P. Magleby, and Larry L. Howell. Zero torque compliant mechanisms employing pre-buckled beams. *Journal of Mechanical Design, Transactions of the ASME*, 142(11):1–12, 2020.

[45] P. Reinier Kuppens, Just L. Herder, and Nima Tolou. Permanent Stiffness Reduction by Thermal Oxidation of Silicon. *Journal of Microelectromechanical Systems*, 28(5):900–909, 2019.

[46] Armin Numic, Thijs Blad, and Fred van Keulen. Stiffness compensation through matching buckling loads in a compliant four-bar mechanism. *Journal of Mechanisms and Robotics*, pages 1–23, 2021.

[47] M. Mariello, T. W.A. Blad, V. M. Mastronardi, F. Madaro, F. Guido, U. Staufer, N. Tolou, and M. De Vittorio. Flexible piezoelectric AlN transducers buckled through package-induced preloading for mechanical energy harvesting. *Nano Energy*, 85(December 2020):105986, 2021.

[48] A. G. Dunning, N. Tolou, P. P. Pluimers, L. F. Kluit, and J. L. Herder. Bistable compliant mechanisms: Corrected finite element modeling for stiffness tuning and preloading incorporation. *Journal of Mechanical Design, Transactions of the ASME*, 134(8), 2012.

[49] Hom Shen Hsieh and Jehnming Lin. Study of the buckling mechanism in laser tube forming with axial preloads. *International Journal of Machine Tools and Manufacture*, 45(12-13):1368–1374, 2005.

[50] Weiqun Liu, Fabien Formosa, Adrien Badel, and Guangdi Hu. A simplified lumped model for the optimization of post-buckled beam architecture wideband generator. *Journal of Sound and Vibration*, 409:165–179, 2017.

[51] Stephen P. Timoshenko and Gere James M. Theory of elastic stability timoshenko.pdf.

[52] Ali H. Nayfeh and Samir A. Emam. Exact solution and stability of postbuckling configurations of beams. *Nonlinear Dynamics*, 54(4):395–408, 2008.

[53] Nima Tolou, Vincent A. Henneken, and Just L. Herder. Statically balanced compliant micro mechanisms (sb-mems): Concepts and simulation. *Volume 2: 34th Annual Mechanisms and Robotics Conference, Parts A and B*, 2010.

[54] Xingtian Liu, Xiuchang Huang, and Hongxing Hua. On the characteristics of a quasi-zero stiffness isolator using Euler buckled beam as negative stiffness corrector. *Journal of Sound and Vibration*, 332(14):3359–3376, 2013.

[55] Chundong Xu, Zhu Liang, Bo Ren, Wenning Di, Haosu Luo, Dong Wang, Kailing Wang, and Zhifang Chen. Bi-stable energy harvesting based on a simply supported piezoelectric buckled beam. *Journal of Applied Physics*, 114(11):1–6, 2013.

[56] Jiantao Zhang, Jia Zhang, Chang Shu, and Zhou Fang. Enhanced piezoelectric wind energy harvesting based on a buckled beam. *Applied Physics Letters*, 110(18), 2017.

[57] Pengcheng Jiao, Wassim Borchani, Hassene Hasni, and Nizar Lajnef. Enhancement of quasi-static strain energy harvesters using non-uniform cross-section post-buckled beams. *Smart Materials and Structures*, 26(8):085045, 2017.

[58] T W A Blad. Whitepaper : MATLAPDL Control Panel – A MATLAB interface. pages 1–6, 2021.